Stony Brook University

Modeling of Air-Droplet Interaction, Substrate Melting and Coating Buildup in Thermal Spraying

A Dissertation Presented

by

Guanghua Wei

to

The Graduate School

in Partial Fulfillment of the

Requirements

for the Degree of

Doctor of Philosophy

in

Mechanical Engineering

Stony Brook University

December 2007

Stony Brook University

The Graduate School

Guanghua Wei

We, the dissertation committee for the above candidate for the
Doctor of Philosophy degree,
hereby recommend acceptance of this dissertation.

Dr. Hui Zhang, Advisor
Mechanical Engineering Department

Dr. Lili Zheng, Chair
Mechanical Engineering Department

Dr. Chad S. Korach, Member
Mechanical Engineering Department

Dr. Andrew Gouldstone, Outside Member
Materials Science and Engineering Department

This dissertation is accepted by the Graduate School

Lawrence Martin
Dean of the Graduate School

Abstract of the Dissertation

Modeling of Air-Droplet Interaction, Substrate Melting and Coating Buildup in Thermal Spraying

by

Guanghua Wei

Doctor of Philosophy

in

Mechanical Engineering

Stony Brook University

2007

Among the many surface coating techniques now available, thermal spray is known to offer the most advantages. It can meet a wide range of technical and engineering requirements in a relatively inexpensive and easily controllable way with the capability of producing repeatable results. In the last few decades a lot of important strides have been made in the field of measurements and modelling of thermal spraying. However, due to the complex of the process and the lack of basic materials-based knowledge about the particle melting, spreading and deposition, the relationship between the process parameters and the coating properties still remains unclear. In thermal spraying, a particle is melted to form a droplet with morphology and thermal- and kinetic-energy status change by the interaction with the plasma/flame. In order to produce higher-quality

coatings and expand the use of this versatile family of technologies, modelling of the particle behaviors during in-flight, spreading and deposition is essential.

This thesis investigates the connections between particle characteristics and coating properties. Momentum, heat and mass transfer phenomena related to particle in-flight, droplet impacting, spreading, and splat layering are studied. Numerical models are developed to establish the quantitative relationships between spray parameters, particle and substrate properties and deposition characteristics.

Most existing theoretical studies of in-flight particle assume that the particle is in a spherical shape without voids inside. The behavior of porous particles in thermal spray has not been well understood. However, the presence of voids in the feedstock powders may have a great impact on particle in-flight behaviors such as particle acceleration, melting and oxidation because a hollowed particle is also lighter than a densed one and this will affect the particle trajectory. The particle shape also needs to be taken into account because it influences the drag force and particle feeding velocity. In this thesis, the level set method is used to study the interaction between the droplet and the surrounding air. The level set function is used to track the deformation of the free surface. The capability of this model on accurately and efficiently simulating the droplet deformation and oscillation is demonstrated. The droplet deformation during in-flight caused by the air-droplet interaction and the droplet-substrate interaction are considered here. Particles with different surface tension and morphologies are studied as well.

Droplet substrate interaction is studied to understand the substrate melting behavior. A numerical model is developed to investigate the droplet solidification, substrate melting and re-solidification. A dimensionless parameter, “temperature factor”,

is proposed from analysis and it can be used as an indicator to predict whether substrate melting will occur for a certain combination of the droplet and substrate. This parameter can be correlated with the maximum melting depth of the substrate. The possibility of heating up the substrate by plasma flame, and attaching a temperature-control device on the backside of the substrate to achieve substrate melting is studied. The substrate front surface temperature can be controlled at a sufficient high temperature. With additional heating from superheated molten droplets and the latent heat of droplet solidification, a thin liquid layer of the substrate can be obtained and epitaxy growth of the splats is possible. This could expand thermal spray technology to the applications of semiconductor and solar energy, both of which need epitaxy crystal with big sizes.

To better control the existing thermal spray process, it is important to develop the quantitative relationships between spray parameters and coating characteristics. Until recently, the simulation studies have been focused on two-dimensional models and prediction of the cross-section structure of deposited layers; although a few three-dimensional models are developed as well by using the statistical particle parameters as input. However, all these models failed to connect the process parameters to coating properties. The coating deposition study here focuses on the development of a computational model, which is able to build a relationship between the process parameters and the coating properties by using the particle data from LAVA 3D calculation results, and to simulate the deposition together with the porosity evolution inside the coating. We propose a set of coating build-up rules to predict the coating deposition and the pore formation, considering the influences of particle size, velocity and temperature and impact position.

To my parents

Table of Contents

List of Figures

List of Tables

Nomenclature

b	thickness of the splat
Cp	specific heat (J/kgK)
d	particle/droplet diameter
D	splat diameter
f	a contact factor
F	volume fraction
Fr	Froude number $Fr = u^2 / gL$
L	latent heat
h	heat transfer coefficient
H	Heaviside function
h_f	latent heat (Jkg^{-1})
Ja	Jacob number, $Ja = c_1(T_m - T_B) / h_f$
k	thermal conductivity ($W\,m^{-1}K^{-1}$)
P	particle parameters
Pr	Prandel number, $\mathrm{Pr} = \nu / \alpha = \mu / (\rho\alpha)$
Re	Reynolds number, $\rho u D / \mu$
R	particle radius (μm)
S	solidification thickness
sgn	sign function
t	time
T	temperature (K)

u	velocity (m/s)
V	interface velocity
We	Weber number $We = \rho_1 u^2 L / \sigma$
X	axial coordinate
y	vertical coordinate
Y	axial coordinate; the coating thickness
Z	axial coordinate

Greek symbols

α	thermal diffusivity Thermal diffusivity ($m^2 s^{-1}$)
β	mean value of particle parameters
γ	thermal expansion coefficient
δ	lift gap; the Dirac delta function in LSF
Δ	temperature factor
ε	interface thickness
ξ	spread factor
η	viscosity ratio
κ	free surface curvature
λ	density ratio
μ_k	linear kinetics coefficient
μ	viscosity (kg/ms)
ρ	density Density (kg/m^3)

σ	standard deviation of particle parameters
ϕ	level set function
ψ	stream function
ω	vorticity

Subscripts

0	initial substrate temperature
i	interface
in	inner size of hollowed particle
j	phase(solid or liquid)
L	liquid
m	melt
out	outer size of hollowed particle
p	initial splat temperature
S	solid
SB	bottom surface of the splat
sp	splat
ST	top surface of the substrate
sub	substrate
B	bottom of the splat

Chapter 1 Introduction

1.1 Thermal Spray Process

Thermal spraying is a group of coating processes in which finely divided metallic or nonmetallic material is deposited in a molten or semi-molten condition to form a high performance coating, offering protection from wear, extreme temperature, chemical attack and environmental corrosion. The coating material may be in the form of powder, rod, wire, or molten materials (Hermanek 2001). Typically there are two categories based on the spray energy sources as illustrated in Figure 1.1, in each category there are a few thermal spray processes that are widely used today.

Thermal spraying has been used for almost 100 years. This field has been developing quickly since 1911, when Dr. Max Ulich Schoop from Zurich, Switzerland applied low melting-point materials, such as tin and lead, on metal surfaces to form coatings by flame spraying to enhance corrosion performance. Early thermal spray processes were used for melting and depositing metals. To avoid unmelted particles in the spray jet, wire – flame spraying was developed, but the material's melting temperature was still limited around 1500^{o}C.

Applications for ceramics and other materials were introduced in the 1950s. Thermal Dynamic Corp. (Lebanon, NH) (Fauchais, Vardelle et al. 2001) invented plasma spray torches in 1957. First it was used for the aeronautics industry, which includes NASA, and later in the aircraft industry. This extended thermal spray technology to any material that could melt. The invention of vacuum plasma spraying (VPS) and low pressure plasma spraying (LPPS) was in the 1980s. Today plasma spray may be the most common method by which thermal sprayed coatings are applied. This cost-effective process is an excellent fit for applications where substantial amounts of material must be applied and where extremely low porosity is not a priority.

Almost at the same time as when plasma spray was invented, Union Carbide Corporation (now Praxair Surface Technologies, INC., Indianapolis, IN) marketed Detonation-gun producing premium coatings in 1950s, especially metallic and cermet ones. In 1980s the High Velocity Oxifuel Flame (HVOF) technique was introduced, in which high pressure was produced continuously by combustion in a water-cooled chamber, from where the gases expanded through a nozzle and accelerated to atmosphere (Fauchais, Vardelle et al. 2001).

In the last few decades thermal spray technology has been a virtual revolution in the capability of technology to produce high performance coatings for a great range of materials on different substrates. Future development will include improved on-line real-time feedback control, intelligent SPC (Statistical Process Control, using statistical techniques for measuring and improving the quality of processes), design of new equipment and spray powders, as well as 3D-process modeling. Improved understanding of the complex nonlinear physics underlying plasma spray process is needed.

Of the many surface techniques now available, thermal spray is known to offer the most advantages. It can be used to satisfy a wide range of requirement, relatively inexpensive, easily controlled and capable of producing repeatable results. Industries around the world are creating extraordinary, high-performance components with the help of thermal spray technology. By changing the surface properties, thermal spraying technology is used to produce high performance coatings of a wide range of materials, e.g. ceramics, metallics, polymers and composites etc., on different substrates or surfaces providing protection from wear, extreme temperatures, chemical attack, and environmental corrosion; and enhancing or decreasing thermal or electrical conduction. It is receiving substantial attention in research, manufacturing, production and service industries as an efficient and cost effective means for the processing of high performance coatings and functional surfaces.

The following are some of the benefits of thermal spray coatings:

(1) Versatility. The thermal spray process offers industrial design engineers maximum flexibility-from the nearly unlimited usable materials selection to the high degree of control over other variables. Almost any metal, ceramic, or plastic can be sprayed. (2) Improves part performance by applying coatings that dramatically increase the useful life of critical parts; (3) Reduces manufacturing costs. Instead of making the entire part out of an expensive material, a high-performance material is sprayed onto a low-cost base material. (4) Repair worn parts and those damages in service, and restore dimensions to mis-machined parts. (5) Creates competitive advantages by creating component parts with unique technological features; (6) Eliminate manufacturing

processes like heat treating and chrome plating and reduces finding/machining operations; (7) Increase component life.

In general, thermal spray coatings of high performance materials, such as metals, alloys, ceramics, or cermets are applied to relatively easy to work and more economical base materials. The combination of coating and base-material can be tailed to provide resistance to heat, wear, erosion, and/or corrosion, as well as other unique sets of surface characteristics.

1.2 Studies in Thermal Spray Process

Thermal spray is a continuous melt-spray deposition process, in which particles in the range of 1-70 microns in diameter are heated, melted (partially or fully), propelled and impacted onto a prepared substrate. The process involves the generation of a stable high temperature plasma/combustion jet (rapid heating); heating and acceleration of powder particles injected into the jet; high velocity impact, subsequent spreading, rapid cooling and solidification of splats, and deposition of numerous droplets. The momentum, heat and mass transfer phenomena govern this deposition process and the mechanical and thermal properties of the coating depend on the control of these phenomena. Lots of work (Lavernia and Grant 1988; Boulos, Fauchais et al. 1994; Waldvogel and Poulikakos 1997; Zhang 1999; Zhang, Wang et al. 2004) has been done

to improve the knowledge in the heat, mass and momentum transfer involved in thermal spray as well as industry processes, especially in plasma spray and HVOF spray.

In the last few decades a lot of important strides have been made in the field of measurements and modelling (Madejski 1976; McPherson 1981; Lavernia and Grant 1988; Fauchais, Coudert et al. 1992; Wang and Matthys 1992; Vardelle, Vardelle et al. 1995; Herman and Sampath 1996; Jiang, Matejicek et al. 1999; Zhang 1999; Wang, Prasad et al. 2001; Zhang, Wang et al. 2004; Li and Christofides 2005; Dyshlovenko, Pawlowski et al. 2006). They allow us to understand the interactions between the flame and particle, splat and substrate, and splat and splat better. However, the principal limitation of thermal spray is the lack of basic materials-based knowledge of the melting, spreading, deposition, and relationship of these to complex process parameters involved. For instance, understanding of the relations between operating conditions and microstructure formation, as well as influence of microstructure on properties/behaviors, i.e., coating formation, is still poor although many studies have been performed. Lack of such fundamental structure property relationship makes it difficult to understand the coating process.

In thermal spray process the time scales for the most events are in the microsecond regime (Fauchais 2004), and the overall process operates thus principally in the region of non-equilibrium and rapid solidification. This makes the experimental study of these very tough.

The second reason is that the deposited materials represent a hierarchy of microstructures across various length scales: such as nano-elements, micron-sized grains contained within the mesoscale splat structures and a variety of nano, micro- and meso-

scale defect structures comprising of voids, microcracks and oriented boundaries. Such microstructures offer an exceptional platform to study complex materials and systems that can help develop a profound understanding of the interrelationships between materials, structures and states (Herman and Sampath 1996; Sampath and Herman 1996).

The last reason is that the coating thermo/mechanical properties depend on thermal spray parameters involved in the process. The number of thermal spray parameters involved in the process is around 50~60 (Fauchais 2004). Quantifying the effects of all the parameters is very difficult due to the large number of them, the random and discrete deposition process (Montavon and Coddet 1996). For a modeling approach it is necessary to reduce the great number of influence parameters down to a few dominating ones. The number of dominating parameters for the plasma spray process is still large (around 20) (Lugscheider, Barimani et al. 1996).

Thermal transport phenomena during particle in-flight, droplet impact, spreading and solidification are the essential issues as well as the pileup of the droplets. For better control the existing processes and developing new applications, it is important to discover the quantitative relationships between the spray parameters, the material properties and the deposition characteristics. Theoretical and numerical models provide an efficient way to expand our knowledge about thermal spray processes, which can leads to the improvement of the current technology. Numerical models can scan through parametric space quickly and can isolate the critical parameters that control the microstructures. This offers two main advantages: At first, it allows us to focus the experimental efforts on the region of parametric space that is important; secondly, it allows us to develop a fundamental understanding of the interaction between various parameters in the spray

system (Cirolini, Harding et al. 1991). Modeling can ultimately link spray parameters, particle in-flight behavior, and single splat formation to coating microstructure.

The thermal spray processes can be viewed as three distinct zones: torch, particle in-flight and droplet/substrate interaction regions, as shown in Figure 1.2, the physics phenomena involved in are listed in Figure 1.3 .

An increasing interest has been found in process predictions using modelling in the past few decades (Dykhuizen 1994; Pasandideh-Fard, Bhola et al. 1998; Wan, Prasad et al. 1999; Wan, Zhang et al. 2001; Pasandideh-Fard, Chandra et al. 2002; Fauchais 2004; Zhang, Wang et al. 2004; Li and Christofides 2005; Dyshlovenko, Pawlowski et al. 2006). Thermal spray modelling can be categorized into three areas:

(1) Flame/Plasma Model: includes the torch design, flame/plasma generation, gas flow; thermodynamic and transport properties of flame/plasma;

(2) Particle In-flight Model: includes particle chemical composition, size distribution and morphology; heat and mechanical flame/plasma-particle interactions;

(3) Coating formation model: includes droplet/substrate interaction, microstructure evolution and coating build-up. The related issues are splat spreading, splashing, substrate melting and re-solidification, droplet cooling, solidification, nucleation and crystallization, grain morphology, and coating microstructure.

After a particle has melted to form a droplet, its morphology and thermal- and kinetic-energy status (temperature, velocity) will be changed by the interaction with the plasma/flame. In order to produce higher-quality coatings and expand the use of this versatile family of technologies, the ability to model particle behaviors during in-flight and during deposition is essential.

This thesis aims at the investigation of heat/mass transfer to particle and coating deposition. The momentum, heat and mass transfer phenomena that govern the particle in-flight process, droplet impact and solidification, and splat layering will be studied. Models are developed to build the quantitative relationship between the spray parameters, the particle/substrate materials and deposition characteristics. Modeling study will focus on the melt flow during particle in-flight for particles at different morphologies, its influence on the drag force on the surface and its influence on the particle/droplet morphology before/after impacting on the substrate. The coating deposition study focuses on three parts: splat/substrate interaction, microstructure evolution and coating build-up.

In the following part of this chapter, literature review will be provided on the modeling of particle in-flight, substrate melting and re-solidification, and coating buildup.

1.3 Modeling of Particle In-Flight

The interaction of particles with thermal spray jet is critical in determining the coating properties, which, to a large extent, depend on the particle temperature, velocity and melting status at the instant of impact on the substrate. Therefore, an accurate description of transport phenomena of particles is essential to the improvement and control of the coating quality.

Heat and momentum transfer between a particle and a high temperature flow has received much attention since 1980s (Boulos, Fauchais et al. 1993; Wan, Prasad et al. 1999). Computational models have taken into account many effects (Chen and Pfender 1983; Wan, Zhang et al. 2001) related to thermal spray conditions, e.g., steep temperature gradient, non-continuum effects, and vaporization. A spherical particle without shape deformation is assumed and the particle heat transfer and solidification are usually calculated using either a lumped analysis or one-dimensional analysis. Heat conduction is considered within the droplet together with surface radiation and reaction. Spherical droplets with constant velocity and uniform temperature are usually assumed in these droplet impact simulations, and the droplet-gas interaction is generally neglected (Amon, Schmaltz et al. 1996; Zhang 1999; Zhang, Wang et al. 2001; Wang, Zhang et al. 2002).

Various methods of powder manufacturing have been used to produce micro and nano-structure particles in thermal spraying. For example, the plasma densified process produces hollow spherical powders (HOSP) which have high porosity, as high as 50%. This kind of Zirconia hollow particles is widely used in thermal barrier coatings and the produced coatings have a lower thermal conductivity comparing with the densed particles. Fused and crushed particles (FC) have a more angular and polyhedral shape. The particles made by SG (Sol-gel) technique exhibit spherical/equiaxed morphology, thus leading to higher surface area. The agglomerated and sintered particles (A&S) have globular/rough-textured shape. Powder particles of different morphologies are used in industry (Kulkarni, Wang et al. 2003). Different particle shapes and a wide range of porosities have been found in the products as shown in Figure 1.4.

However, most theoretical studies of in-flight particle physics assume the particle is a spherical shape without voids inside. The behavior of angular and/or porous particles in plasma flame has not been well understood. In fact, the presence of voids in the feedstock powders may have a great impact on particle in-flight behavior such as particle acceleration, melting and oxidation, which are further related to splat formation and coating buildup (Sobolev and Guilemany 1995). Heat flux from the plasma is hampered by the voids, which will influence temperature distribution inside the particles. The porosity will further influence the melting process of the particle. A hollowed particle is also lighter than the densed one; it will affect the trajectory of the particle. The particle shape is also needed to be taken into account because it influences the drag force and particle feeding velocity. Researches (Xu, Wu et al. 2003) noticed that non-spherical particles will experience different heating histories, but very little attention was paid to simulate the hollow particle in-flight and impact due to difficult in the shape change and flow instability.

In particle in-flight simulation, a spherical droplet without deformation is usually assumed and heat transfer and solidification are calculated using either a lumped- or a one-dimensional model. Melt flow and droplet deformation are usually neglected (Amon, Schmaltz et al. 1996; Wang 2002; Xiong, Zheng et al. 2004; Li and Christofides 2005; Shanmugavelayutham, Selvarajan et al. 2006). Although multi-dimensional fluid flow droplet models are available, they can only treat a single or few droplets with simplified assumptions. In the droplet impact simulation, the spherical droplets with constant velocity and uniform temperature are usually assumed as initial conditions, and the droplet-gas interaction is neglected. In the experiments, the melt flow inside the droplet

will influence the shear stress on the droplet surface, and further vary the drag force of the droplet. The liquid droplet will therefore have a lower drag coefficient than the solid one with the same size and velocity. Also, the droplet deformation plays an important role in the droplet velocity and melting. Furthermore, particles with different morphologies, especially, hollow particles, are widely used in industry (Klocher and Clyne 2001). For example, YSZ hollow particles have been used for thermal barrier coating and the produced coatings have a lower thermal conductivity compared with those produced by the densed particles. Very few studies have been performed to understand the particle impact other than the densed, spherical ones (Klocher and Clyne 2003).

During droplet in-flight, the original shape of the particle, and melt flow inside the droplet will influence the shear stress on the droplet surface, and it will further vary the drag force. A molten droplet will experience different thermal- and kinetic histories from a solid one with the same size and injection condition. Also, the shape deformation may play an important role for particle in-flight, and followed impact and solidification processes. To understand such phenomena, we will introduce the level set method to the study of particle in-flight in thermal spraying.

The level set method was developed to model the formation and deformation of bubbles and drops (Osher and Sethian 1988; Sussman, Smereka et al. 1994; Chang, Hou et al. 1996; Chen, Merriman et al. 1997; Zhang, Zheng et al. 1998; Sethian 1999; Zheng and Zhang 2000; Sethian and Smereka 2003; Ohta, Imura et al. 2005). It was first introduced in 1980s (Osher and Sethian 1988). It was widely used because it is simple but versatile for computing and analyzing the motion of an interface in two or three

dimensions. Zhao et al. (Zhao, Merriman et al. 1998) developed a level set approach to simulate the behavior of the bubble and droplet with several phases. Zhang et al. (Zhang, Zheng et al. 1998) developed a level set method together with adaptive grid generation. This scheme is successfully applied to various solidification problems with deformable free surfaces. Zheng et al. (Zheng and Zhang 2000) further extended the model into three-dimension and used to study deformable free surface problem with or without solidification. The model is used to simulate the transport phenomena such as droplet deformation and solidification.

1.4 Substrate Melting and Re-Solidification

In thermal spray processes, the molten or semi-molten droplets impinge on substrate and rapidly solidify to form thin "splats". The coatings are built up by successive impingement and inter-bonding among the splats. Whether the splats will melt the substrate is an import issue in the coating quality.

Various experimental and numerical studies have been conducted to investigate the mechanism of substrate melting and re-solidification. For example, McPherson (McPherson 1981) investigated the metallurgical interaction between the molybdenum splat and steel substrate during flame wire spray process, and its impact on coating mechanical properties. Experimental results showed that the properties of the substrate were the key factors on the bonding quality. Steffens et al. (Steffens, Wielage et al. 1991)

discovered that a better bonding between the deposited layers and substrate could be achieved if the interface temperature is higher than melting temperature of the substrate. Fukumoto and Huang (Fukumoto and Huang 1999) conducted the experiments to study the splat morphology. They found that the splat morphology changed from splash to disk-like shapes if the substrate temperature is beyond a certain value. They defined this value as “transition temperature”. Jiang et al. (Jiang, Matejicek et al. 1999) also observed that the substrate surface temperature in plasma spraying has a profound effect on the splat morphology, and consequently on the microstructure and properties of the deposits. For different splats and substrates, the splat morphology and crate depth are measured (Li, Wang et al. 2004). The results showed that both the particle and substrate materials are important during melting and consequently influence on the bond strength. Above experimental studies confirmed that the interaction between the high melting point deposit and the lower melting point substrate is affected by splat and substrate material properties and temperatures.

Numerical simulations are widely used to investigate the spreading and solidification processes in thermal spraying. Amon et al. (Amon, Schmaltz et al. 1996) developed a numerical model that analyzed the melting of the substrate for a superheated molten droplet impinging on various substrates for micro-casting applications. The model was further modified by Schmaltz et al. (Amon, Schmaltz et al. 1996) and Zaralejo et al. (1999). The critical conditions for the substrate melting were provided in their papers. Chung and Rangel (Chung and Rangel 2001) used the Madjski type model to simulate the droplet deformation and solidification. Energy equation was solved in the entire domain by coordinate transformations. Their model was used to predict the conditions of

substrate melting by comparing substrate surface temperature with its melting temperature. In their model, the perfect contact between the deposited layer and the substrate was assumed. Wang et al. (Wang, Prasad et al. 1997; Wang, Wang et al. 1998) studied both solidification of the deposited layer and mleting of the substrate using non-equilibrium phase change kinetics conditions at the solid-liquid interfaces. An implicit finite difference method with interface tracking was developed. Zhang (Zhang 1999) developed a theoretical model for the splat-flattening ratio accounting for the wetting and solidification of the droplet. Attinger et al. (Attinger and Poulikakos 2001) studied the molten micro-droplet impacted and solidified on a cold flat substrate. Their model was also used to account for substrate melting and re-solidification, with the consideration of interfacial contact resistance and the mixing. Results demonstrated the influence of the droplet fluid dynamics on the substrate melting and re-solidification. Zhang et al. (Zhang, Wang et al. 2001) and Wang et al. (Wang, Zhang et al. 2002) investigated the interaction between the melt flow and rapid solidification of the splat. Substrate melting and droplet splashing were also considered in their papers. The numerical model developed in their papers included the melt flow, movement of free liquid surface, motion of the liquid-solid-air contact line, and non-equilibrium solidification of the droplet. Numerical results revealed that the droplet and substrate temperature played a significant role on substrate melting and droplet solidification. Li et al. examined the role of particle and substrate materials on the substrate melting (Li, Wang et al. 2004), their influence on the maximum melting depth and consequently bonding strength have been discussed numerically and experimentally. Li et al. found that the melting of substrate surface to certain depth alter the flow direction of droplet fluid (Li, Li et al. 2006). The change of fluid flow direction

led to detachment of fluid from contact with the substrate; they also observed that the morphology of splats depends not only on the particle temperature and velocity, but also on thermal interaction between molten particle and substrate.

Melting and re-solidification of the substrate may help coatings to achieve a better bonding with the substrate at some conditions. In other conditions, it may damage the substrate. A good understanding of this phenomenon is essential for appropriate bond coat selection as well as avoiding of substrate damage.

1.5 Coating Build-Up

Thermal spray microstructures are composed of splat-based elements formed through impact and solidification of micro-sized droplets. The splat-based microstructures create a variety of imperfections, which can vary in size, volume density, morphology and orientation. Three principal defect types are present in the system: disk-like lamellar pores, which are formed due to imperfect inter-splat wetting, leading to decreased adhesion between sprayed layers; globular pores formed as the result of lack of filling of the solidifying splat; and vertical micro-cracks in the splat and deposit which contribute to very fine porosity in ceramics. These defects and their related anisotropies affect modulus, fracture toughness, strain hardening, etc., as well as functional attributes, such as, thermal conductivity.

The dominant parameters for coating formation and resulting coating characteristics are the particle characteristics and substrate conditions, e.g., temperature, surface morphology, roughness, and oxidation. Depending on the shape of splats and the nature of their interactions, different types of microstructures, varying porosities, and consequently different coating properties are obtained. Physical mechanism of the thermal spray coating formation is very complex, but significant efforts have been made to simulate the microstructure formation using mathematical model: Knotek and Elsing (Knotek and Elsing 1987) developed a thermal spray deposition model, and they used the Monte Carlo method to predict the size and distribution of cracks and pores in the coatings. Their model was a two-dimensional one, and could only predict the structure of a single cross-section through the deposited layer. Cirolini et al. (Cirolini, Harding et al. 1991) simulated the coating deposition with a two-dimensional stochastic model, and postulated a much more complex set of rules to represent interaction between splat pipe-up process. Hansbo and Nylen (Hansbo and Nylen 1999) developed a model to simulate coating layer build-up and robot motion without any attention to the internal coating microstructure. Chen et al. (Chen, Wang et al. 2001) used a ballistic deposition model to track individual stainless steel powder particles in plasma spraying. They simulated the coating growth and pore formation and used the model to analyze the effects of process parameters, such as gun scanning velocity, spray angle on the coating porosity. Mostaghimi et al.(Mostaghimi, Chandra et al. 2003) defined a 3D model of High Velocity Oxy-Fuel (HVOF) spray coating process to predict coating microstructure (porosity, residual stress, and surface roughness) as a function of spraying parameters (particle size, velocity and impact locations). Mariaux et al. computed the distribution of

particle velocity, temperature, size at impact and predicted the heat transfer to the substrate by plasma jet and particle. By the particle parameters obtained from simulation, they predicted the shape of the coating footprint when the torch and the substrate were fixed (Mariaux, Legros et al. 2003). Shi et al. focused on the modeling of the coating produced by an HVOF process. They used stochastic simulations to explore the coating microstructure evolution. In their model, they considered the velocity, temperature and degree of melting of the powders and characterized the influence of operating conditions, such as the gas flow rate and spray distance, as well as the effect of particle size on melting behaviour, coating porosity, surface roughness, and deposition efficiency (Shi, Li et al. 2004). Dyshlovenko et al. (Dyshlovenko, Pawlowski et al. 2006) simulated the plasma sprayed ceramic particle interaction and coating growth. The particle diameter of the arriving particle was chosen from a suitable distribution. They used a numerical model to determine the velocity and temperature of the particles before impact and use these data to simulate coating porosity and plot in the cross section view.

1.6 Preview of This Thesis

Chapter 2 states the problems in the current study and addresses the research objects of this thesis.

Chapter 3 presents the fundamentals of numerical modeling of air-particle interaction and discusses the preliminary results.

Chapter 4 presents the study of substrate-droplet interaction and results.

Chapter 5 investigates the coating buildup process.

Chapter 6 summarizes the work done and addresses the recommendation for the future work.

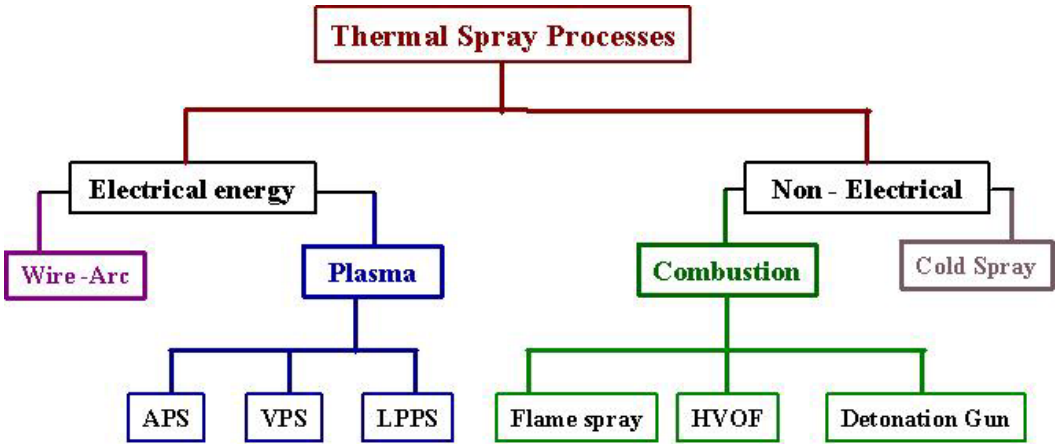

Figure 1.1 Traditional thermal spray processes

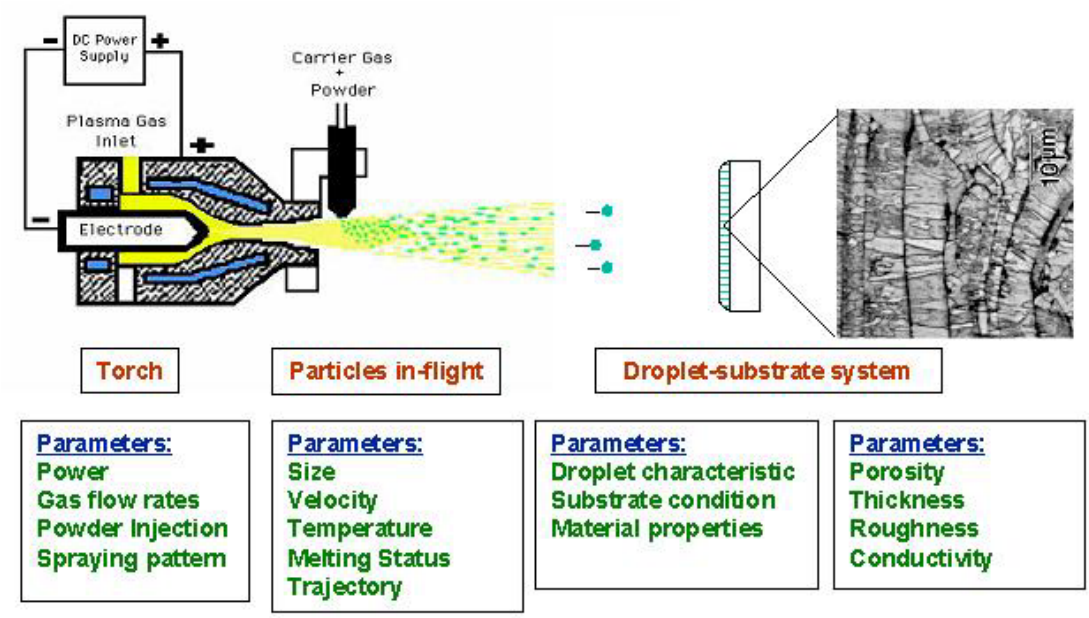

Figure 1.2 Schematic of thermal spray process

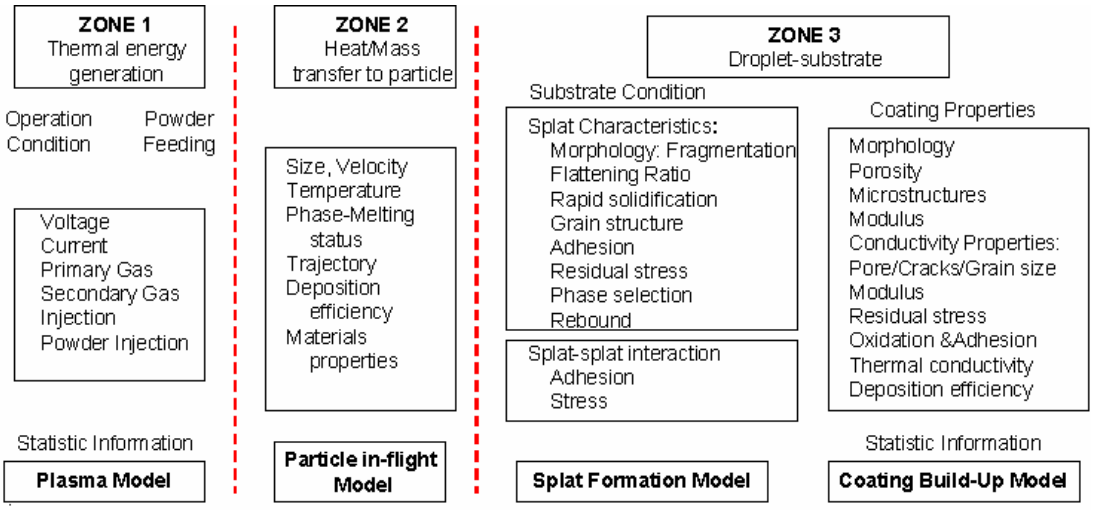

Figure 1.3 Physics and models for thermal spray process

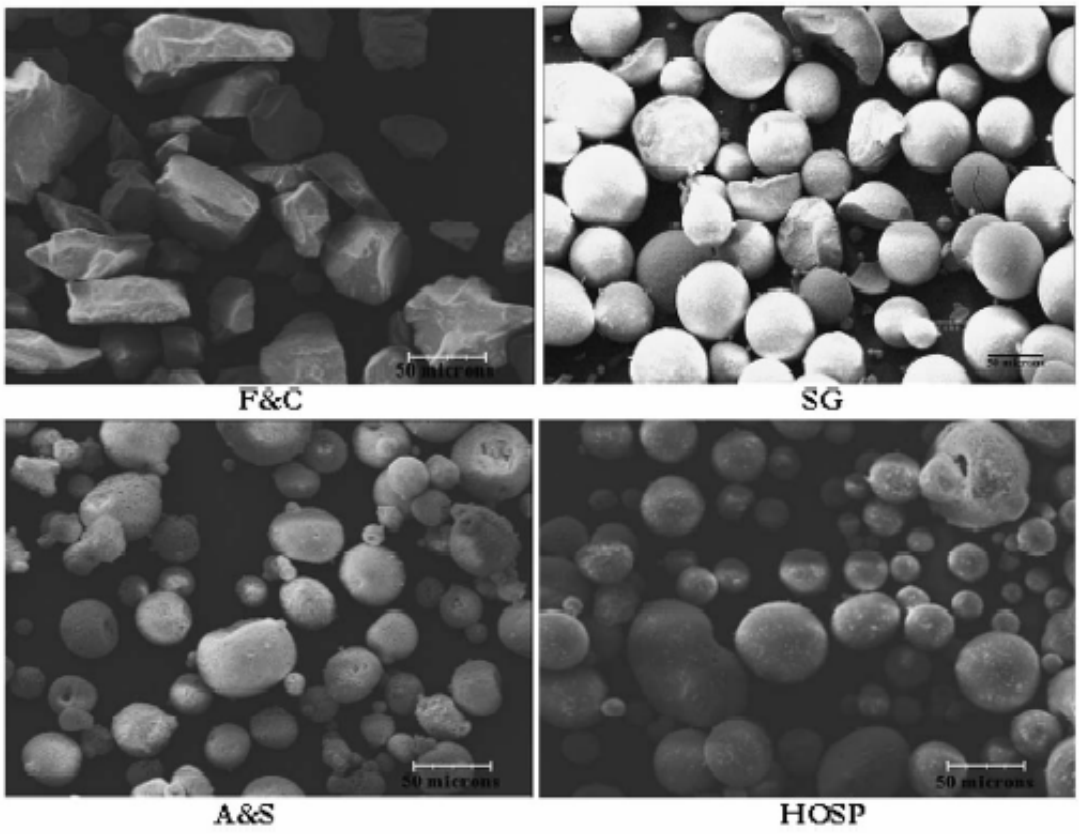

Figure 1.4 PSZ powder powder morphologies observed under SEM (50 μm scalebar)(Kulkarni, Wang et al. 2003)

Chapter 2 Research Objections

2.1 Research Topics

To better control the existing thermal spray process, it is important to develop the quantitative relationships between spray parameters and coating characteristics. This thesis aims to investigate the interactions between droplet characteristics and coating properties. Momentum, heat and mass transfer phenomena govern the particle in-flight behavior, droplet impact and solidification, and splat layering will be studied. Numerical models are developed to establish the quantitative relationships between spray parameters, particle and substrate material properties and deposition characteristics. Modeling work will focus on the melt flow in the droplet during in-flight of the particles of different morphology, and its influence on the drag force and splat formation; Droplet substrate interaction study will focus on the substrate melting behavior, rapid solidification and grain structure; The coating deposition will focus on developing a computational model to predict the layering process and coating porosity evolution.

2.2 Modeling of Particle In-Flight

Modeling of droplet deformation during in-flight and impact poses a great challenge to numerical analysts and computational scientists. The volume tracking method, such as volume of fluid (VOF) scheme is widely used to simulate a single droplet spreading and solidification on a flat or waved substrate. The VOF method is easy to use and implement, but it suffers from low accuracy and numerical instability. Beside the VOF method, the level set method is another choice for simulation of droplet in-flight, splat spreading and solidification.

In this thesis, the level set method will be used to study the interaction between droplet and surrounding air and understand the air-trapping mechanism. The level set function will be used to track the deformation of the droplet free surface. The capability of the model on accurately and efficiently simulating the droplet deformation and oscillation will be demonstrated and research will focus on the melt flow inside the droplet caused by air friction, and instability caused by the droplet-air interaction and droplet-substrate interaction. Particles with different sizes and morphologies are studied for plasma spray application.

2.3 Substrate Melting and Re-Solidification

Melting and re-solidification of the substrate during droplet impact plays an important role in adhesion and material strength. Whether the splats will melt the substrate is an important indication in the coating quality. This is also an important issue for many other applications such as ink-jet painting, micro-soldering, high temperature casting where droplets may melt the pre-deposited material. It is necessary to know the mechanism of substrate melting and its influence on coating properties, and good understanding will help us optimize the coating properties.

A numerical model will be developed to investigate the solidification of the droplet, and melting and re-solidification of the substrate. The solidification interface movement can be obtained by applying a rapid solidification model on the solid/melt interface. Numerical simulations will be used to study the influence of materials and temperatures of splat and substrate on substrate melting and re-solidification. A dimensionless parameter, temperature factor, is proposed from analysis and it will be used as an indicator on whether substrate melting will occur for a certain combination of the droplet and substrate, and this parameter can be correlated with the maximum melting depth of the substrate.

By heating up the substrate by plasma flame with a temperature-control device at the substrate backside to achieve substrate melting was studied. The substrate front surface temperature can be controlled at a certain high temperature together with the heating from superheated molten droplets and the latent heat of droplet solidification, a thin liquid layer of the substrate can be obtained. Particle melting status, particle velocity, particle surface temperature, and controlled substrate backside temperature are important

for substrate melting. It is therefore possible to make epitaxial splat deposition, and broader new applications will be possible to find.

2.4 Coating Build-Up

The splat-based coating microstructures create a variety of imperfections, which can vary in size, volume density, morphology and orientation. These defects and their related anisotropies affect modulus, fracture toughness, strain hardening, as well as thermal conductivity. The dominant parameters for coating formation and coating characteristics are the particle characteristics and substrate conditions. Depending on the shape of splats and the nature of the interaction, different types of microstructures, varying porosities, and consequently different coating properties are obtained.

The physical mechanism by which thermal spray coating is formed is complex. Almost all the attempts in the literature have their limitations. Some research focuses on two-dimensional models, and predicts the cross-section structure of deposited layers; the other is developed a three-dimensional model and used the statistical particle parameters as input. All the models failed to connect the process parameters to coating properties. It is evident that a detailed computational model of splat-splat interaction is desirable to obtain the porosity, surface roughness and thickness of the coating considering splat adhesion and quenching stresses. This will form the foundation for further improvement of the advanced coating build-up model.

In this thesis, the results of a comprehensive three-dimensional computational code (LAVA3D-P) are used as the coating buildup input data, which includes the particle status and trajectory. Mean values and standard deviations of particle size, velocity, and temperature, and impact position are obtained from in-flight particle simulations. These spray parameters controlled droplet characteristics together with the given substrate conditions are used as initial conditions of splat morphology predictions and in turn as the input for coating buildup. We propose a set of coating build-up rules to predict coating deposition and formation of the pores, considering the influences of particle size, velocity, temperature and location related to the substrate.

Chapter 3 Modeling of Particles In-Flight

3.1 Introduction

Different particle sizes and shapes have been used in thermal spraying. However, most theoretical and numerical studies of in-flight particle assume that the particles are spherical shape. In fact, the irregular shape and presence of pores may have a great impact on particle acceleration, trajectory, melting, and oxidation, which are related to the splat formation and coating microstructure. Figure 3.1 showed four different partially-stabilized zirconia (PSZ) particle morphologies. Splat shapes are very different. The disk-shaped splat using the F&C feedstock suggests complete particle melting, resulting in well adhesion between splat and substrate, while the splats are fragmented in splats generated by A&S feedstock. Figure 3.2 shows the significant difference in coating microstructure produced by four kinds of feed stock and Figure 3.3 shows the coating porosity results measured by SANS (small angel analysis system). Experimental results show that particle morphology plays an important role on the splat morphology and coating properties. It is therefore important to understand the effects of particle sizes and

shapes on the splat formation and coating buildup. At the first step, we will study the role of particle shape and geometry on the particle in-flight behavior.

In the in-flight simulation, a spherical droplet without deformation is usually assumed. Heat transfer and solidification are calculated using either a lumped model or a one-dimensional model. The melt flow and droplet deformation for the particle in flight are usually neglected. In the droplet impact simulation, spherical droplets with constant velocity and uniform temperature are usually assumed as initial conditions. During the droplet in-flight, melt flow inside the droplet will influence the shear stress on the surface, and it will further vary the drag force. Also, the shape deformation will play a key role during in-flight and after impact. The presence of pores in the feedstock particle may have a great impact on the in-flight behavior such as particle velocity, melting and oxidation (Sobolev and Guilemany 1995). Researchers (Xu, Wu et al. 2003) noticed that non-spherical particles will experience different heating histories, but very few studies were performed to study the hollow particle in-flight and after impact due to difficult in the shape changes and flow instability.

In this chapter, the level set function will be used to track the deformation of the droplet free surface. The model is used to study the melt flow inside the droplet, deformation of the droplet, and instability of the droplet. The hollowed or densed particle melting, free surface deformation, followed impact and spreading will be simulated. The effects of droplet size and morphology on free surface deformation will be investigated.

3.2 Mathematical Model

3.2.1 Fundamental of the Level Set Method

Moving interfaces, including free surface and solidification, are widely occurred in materials processing. The level set method has been developed to deal with interface tracking. It has been widely used to model the deformation and dynamics of bubbles and drops (Osher and Sethian 1988; Sussman, Smereka et al. 1994; Chang, Hou et al. 1996; Chen, Merriman et al. 1997; Zhang, Zheng et al. 1998; Sethian 1999; Zheng and Zhang 2000; Sethian and Smereka 2003; Ohta, Imura et al. 2005).

The level set method was initially developed in 1980s (Osher and Sethian 1988) to study the problems that need to track the motion of a front whose speed depends on the local curvature. It was widely used because it is simple but versatile for computing and analyzing the motion of an interface in two or three dimensions. Zhao et al. (Zhao, Merriman et al. 1998) developed a level set method to simulate the behavior of the bubble and droplet with several phases. Zhang et al. (Zhang, Zheng et al. 1998) developed a numerical scheme using the level set method together with multizone adaptive grid generation (MAGG). Their method is successfully applied to various solidification problems with deformable free surface. Zheng et al. (Zheng and Zhang 2000) further extended this model into three dimension and used to study the deformable free surface problems with or without solidification. The model is used to simulate transport phenomena in droplet deformation and solidification.

In the level set method, the interface motion is calculated through a scalar variable, the level set function. The interface location is represented by the zero level set function. The interface velocity can be related to the interface position, the interface geometry, surface tension. The level set method can be coupled to a wide variety of problems involving external physics such as: compressible and incompressible (possibly reacting) flow; Stefan problems; kinetic crystal growth; epitaxial growth of thin films; vortex-dominated flows; and multiphase flows. The main application to fluid mechanics is to track an evolving interface. This is done by viewing the boundary as an interface, and then using the level set method to track the moving boundary. The advantages of this approach include: (a) It is easy to evaluate quantities such as the local curvature which determines the surface tension of the interface separating different fluids; (b) Because of the ability of these techniques to allow topological changes in the evolving front, differing regions can merge and split apart; and (c) the approach is unchanged in three dimensions.

3.2.2 Level Set Function

Initial level set function $\phi(x,t)$ defines different values for different fluids: one is positive and another is negative, as shown in Figure 3.4; at the interface of two kinds of fluid $\nabla\Omega$ is modeled as the value of ϕ is zero. The level set function ϕ has the following properties:

$$\phi(x,t)\begin{cases} > 0 & \text{if } x \in \Omega \\ < 0 & \text{if } x \in \overline{\Omega} \\ = 0 & \text{if } x \in \partial\Omega = \Gamma(t) \end{cases} \qquad \textbf{(3-1)}$$

The interface can be captured for all the later time by locating the set $\Gamma(t)$ for which ϕ vanishes. Note that ϕ=0 may define more than one interface if there are breaking, merging and reconnection. Since the interface moves with the fluid, the evolution of ϕ is given by:

$$\frac{\partial \phi}{\partial t} + \vec{u} \cdot \nabla \cdot (\phi) = 0 \qquad \textbf{(3-2)}$$

The whole domain of interest can be treated as one domain; the regions of different fluids or phases can be distinguished by the level set function distribution.

3.2.3 Governing Equations

The governing equation for mass conservation in incompressible fluid as:

$$\nabla \cdot \vec{u} = 0 \qquad \textbf{(3-3)}$$

The governing equation for the fluid velocity $\vec{u}$, along with the boundary conditions can be written as a single equation (Chang, Hou et al. 1996):

$$\rho(\phi)(\vec{u}_t + \vec{u} \cdot \nabla \vec{u}) = -\nabla p + \rho(\phi)\vec{g} + \nabla \cdot (2\mu(\phi)\vec{D}) + \sigma\kappa(\phi)\delta(\phi)\nabla\phi \qquad \textbf{(3-4)}$$

where, $D = \left[\nabla \vec{u} + (\nabla \vec{u})^T\right]/2$. ϕ is the level set function, and the fluid interface corresponds to the zero level set of ϕ, which is governed by the following equation:

$$\partial\phi/\partial t + \vec{u} \cdot \nabla \cdot (\phi) = 0 \qquad \textbf{(3-5)}$$

where δ is the Dirac delta function, and κ is the free surface curvature, which can be expressed by the level set function and its derivatives:

$$\kappa(\phi) = -\frac{\phi_y{}^2\phi_{xx} - 2\phi_x\phi_y\phi_{xy} + \phi_x{}^2\phi_{yy}}{\left(\phi_x{}^2 + \phi_y{}^2\right)^{3/2}} \quad \textbf{(3-6)}$$

In the momentum equation, the last term is the effect of surface tension. ρ and μ are the density and viscosity respectively. Since the density and viscosity are constant in each fluid, they can take on two different values depending on the sign of ϕ:

$$\rho = \rho_1 + (\rho_2 - \rho_1)H(\phi(x)) \quad \textbf{(3-7)}$$

$$\mu = \mu_1 + (\mu_2 - \mu_1)H(\phi(x)) \quad \textbf{(3-8)}$$

where $H(\phi)$ is the Heaviside function given by:

$$H(\phi) = \begin{cases} 0 & \text{if } \phi < 0 \\ 1/2 & \text{if } \phi = 0 \\ 1 & \text{if } \phi > 0 \end{cases} \quad \textbf{(3-9)}$$

3.2.4 Dimensionless Form

The governing equations can be non-dimensionalized based on the following dimensionless variables.

$$\vec{x} = Lx' \quad \vec{u} = Uu' \quad t = (L/U)t' \quad \mu = \mu_1\mu' \quad \rho = \rho_1\rho' \quad p = p'\rho_1U^2 \quad g = g_0g'$$

where the primes denote dimensionless variables. By substituting these variables into Equations (3-3) and (3-4), and dropping the primes, we have:

$$\nabla\vec{u} = 0 \quad \textbf{(3-10)}$$

$$\frac{\partial \vec{u}}{\partial t} + u \cdot \nabla u = -\frac{\nabla p}{\rho(\phi)} + \frac{1}{Fr}\vec{g} + \frac{1}{\rho(\phi)\,\mathrm{Re}} \nabla \cdot \left(2\mu(\phi)\vec{D}\right) + \frac{\kappa}{\rho(\phi) We}\delta(\phi)\nabla\phi \qquad \textbf{(3-11)}$$

where, the Reynolds number, $\mathrm{Re} = \rho_1 UL / \mu_1$, the Froude number, $Fr = U^2 / gL$, the Weber number, $We = \rho_1 U^2 L / \sigma$, and σ is surface tension coefficient.

The density and the viscosity respectively are now

$$\rho(\phi) = \lambda + (1 - \lambda) H(\phi) \qquad \textbf{(3-12)}$$

$$\mu(\phi) = \eta + (1 - \mu) H(\phi) \qquad \textbf{(3-13)}$$

where is $\lambda = \rho_1 / \rho_2$ the density ratio and is $\eta = \mu_1 / \mu_2$ is the viscosity ratio.

3.3 Numerical Scheme

3.3.1 Numerical Algorithm

The numerical algorithm can be outlined as follows:

Step 0: Initialize velocity field and level set function

For a given interface Γ, an associated level set function ϕ can be inialized. If necessary, the re-initialization step described in step 3 can be applied globally to set ϕ be a signed distance function to Γ.

Step 1: Compute velocity field

Calculate velocity from ϕ or the physical problem coupled with ϕ on or near zero level set of ϕ (interface). Using 2nd order ENO upwind scheme for convective terms and central difference scheme for viscous and curvature terms.

Step 2: Interface advancing

Update ϕ near the zero level set function for one time step to get ϕ_0. The new interface position is now equal to the zero level set of ϕ, denote this updated ϕ as ϕ_0 (note that ϕ may not be a distance function at this time)

Step 3: Re-initialization of level set function

Apply the re-initialization step to ϕ_0 in the zone near the zero level set function. Set it to be an exact signed distance function by solving the equation $\frac{\partial \phi}{\partial t} = \text{sgn}(\phi_0)(1 - |\nabla \phi|)$ to steady state, here $\phi(x,0) = \phi_0(x)$.

Step 4: repeat step1 to step 3 to get the next updated value of ϕ.

3.3.2 Thickness of the Interface

In order to solve equation (3-11) numerically we must modify it slightly due to the sharp change in ρ and μ across the front and also due to the numerical difficulties presented by the Dirac delta function. To alleviate this problem we shall give the interface a fixed thickness ε that is proportional to the spatial mesh size. This allows us to replace $\rho(\phi)$ and $\mu(\phi)$ by smoothed variables $\rho_\varepsilon(\phi)$ and $\mu_\varepsilon(\phi)$ and are given by regularized density function and regularized viscosity as:

$$\rho_\varepsilon = \rho_1 + (\rho_2 - \rho_1) H(\phi(x)) \tag{3-14}$$

$$\mu_\varepsilon = \mu_1 + (\mu_2 - \mu_1) H(\phi(x)) \tag{3-15}$$

First we should introduce regularization for the singular Dirac delta function $\delta_\varepsilon(x)$,

$$\delta_\varepsilon(x) = \begin{cases} \dfrac{1 + \cos(\pi x / \varepsilon)}{(2\varepsilon)} & \text{if } |x| < \varepsilon, \\ 0 & \text{otherwise} \end{cases} \tag{3-16}$$

With this regularization, the resulting evolution equations are well posed. We can consider ρ and μ as smooth variable density and variable viscosity. Then the second-order projection method for variable density problems introduced in (Chen, Merriman et al. 1997) can be used to discretize the momentum equations. Some implementation issues for applying the projection method to the level set formulation are discussed in the literature (Sussman, Smereka et al. 1994).

We define the corresponding regularize Heaviside function $H_\varepsilon(x)$ as:

$$H_\varepsilon(x) = \begin{cases} 0 & \text{if } x < -\varepsilon, \\ (x + \varepsilon)/(2\varepsilon) + \sin(\pi x / \varepsilon)/2\pi & \text{if } |x| \le \varepsilon, \\ 1 & \text{if } x > \varepsilon \end{cases} \tag{3-17}$$

The above Heaviside function satisfies the relation $dH_\varepsilon(x)/dx = \delta_\varepsilon(x)$. In our calculation we use $\varepsilon = \frac{3}{2}\Delta x$. Eqs. (3-16) and (3-17) are used to define the corresponding regularized density function and regularized viscosity.

3.3.3 Re-initialization of Level Set Function and Mass Conservation

Zhang (Zhang, Zheng et al. 1998) have developed a high resolution computer model that combine the 2D MAGG, curvilinear finite volume discretization, and level set method to simulate the transport phenomena associated with moving interfaces. The grid generation scheme has been devised for fast and accurate tracking of the interface movement, as well as for clustering grids in the interface regions as the solutions progress.

The equations are solved by a second order ENO (Essentially Non-Oscillatory) scheme (Harten, Engquist et al. 1987) to reduce the numerical diffusion on the free surface. The free surface is updated based on the zero set of the level set function and the surface tension is taken onto account by adding a singular Delta function in the momentum equation (Chang, Hou et al. 1996). Initially, the level set function is set as a signed distance from the interface. In the case of computations for large times, it does not remain a distance function at the later times, and therefore, re-initialization is a critical step in the implementation of the lever set method. Another important issue is the mass conservation. Numerical discretization of the level set formulation does not guarantee mass conservation even with the above re-initialization procedure. To overcome the difficulty a second re-initialization procedure has been employed to preserve the total mass (both liquid and gas) in time (Zhang, Zheng et al. 1998). A method proposed by Sussman *et al.* (Sussman, Almgren et al. 1999) is used here, which can keep ϕ as a signed distance from the front at all the times. This is accomplished by solving the following equation to steady state:

- Does not remain a distance function at the later times, and therefore, re-initialization is a critical step in the implementation of LSM.
- Keeping the level set function as a distance function will ensure that the front has a finite thickness of order ε for all the time.
- Given a level set function Φ=0 at time t, solve for the steady state solution of the equation:

$$\frac{\partial \phi}{\partial t} = \text{sgn}(\phi_0)(1 - |\nabla \phi|) \quad \textbf{(3-18)}$$

The solution of ϕ will have the same sign and the same zero level set as ϕ_0, and will satisfy $|\nabla \phi| = 1$. It is therefore a distance function from the front. Since the initial guess is often close to the signed-distance function, only a few iterations are required to obtain convergence, at least for the class of problems considered here.

For in-compressible flows, the total mass is conserved in time. However, the numerical discretization of the level set formulation does not preserve this property in general. Even the above re-initialization process can not guarantee the mass conservation and the predication of the interface topography can degrade. Therefore, a second re-initialization procedure is devised, with a goal of preserving the global mass at each time step. This requires solution of the following equation to steady state:

$$\frac{\partial \phi}{\partial t} + [A_0(t) - A(t)](-P + \kappa)|\nabla \phi| = 0 \quad \textbf{(3-19)}$$

$$\phi(x,0) = \phi_0(x) \quad \textbf{(3-20)}$$

where $A_0(t)$ is the total mass for the initial condition, which can be calculated, based on the total mass balance and the movement of the interface; $A(t)$ is the total mass corresponding to the level set function $\phi(t)$ in the above re-initialization process. P is a positive constant, which helps stabilize this re-initialization procedure.

3.4 Numerical Results and Discussion

We will use the developed numerical model to study the droplet-air interaction during in-flight and after impact. The free surface deformation of the densed or hollowed spherical droplet will be investigated. The influence of different particle viscosities is studied and in-flight deformations for hollowed particles with different D_{in}/D_{out} ratios are also compared.

3.4.1 Merge of Free Surface for Two Bubbles

The interaction between two bubbles with different densities under the influence of gravitation is considered by many investigators. It will be simulated first to demonstrate the capability of the code. The density of the bubbles ρ_1 is set to be unity and the density of the fluid outside the bubbles ρ_2 is taken as 10. The bubble and the background are rest

at the initial. The bubble will move upward due to gravitation force. In the calculation, total 256x256 grids are used. The bubble deformation was shown in Figure 3.5.

From the figure we can see that the smaller bubble moved faster than the bigger one and it finally merged into a bubble at time $t > 0.3$. The location and shape of the free surface obtained in Figure 3.5 are in good agreement with those in Chang, et al. (Chang 1993). The different grid size using 64x64, 128x128 and 256x256 grids have also been tested. It is found that numerical result will be improved when a finer grid is used. The coarse grids will cause the smearing interface at the sharp position. If the detail of the free surface merging is studied, the fine grids have to be used.

3.4.2 Densed Spherical Droplet

Spreading and deposition of a molten droplet on a flat substrate has been widely studied. The difficult is due to moving boundaries, in which both free interface and solidification interface are moved simultaneously. Situation becomes more difficult if surrounding air is interacted with droplet movement. Few studies are available considering three-phase interaction. Particle deformation during in-flight and impact is investigated. To simplify the problem, a molten droplet at zero velocity is assumed to be the initial condition. In the thermal spray experiments, solid particle enters the flame and is heated and melted. Heating and melting processes are neglected here. Research will be focused on the droplet-air interaction. The difference particle during in-flight and spreading behaviors can be investigated. In this study, the grid size of 256x256 is used for all the calculations.

In the simulation, a molten ZrO_2 droplet traveling in the air is considered. The parameters of ZrO_2 and air used in the calculations are shown in Table 1, the calculation results present in Figure 3.6.

Table 1 Parameters of ZrO_2 and air used in the calculation

ZrO_2		
	Diameter(μm)	60
	Velocity(m/s)	100
	Density (kg/m^3)	5.89E+03
	Viscosity (Ns/m^2)	0.008
	Surface tension(N/m^2)	0.3
Air		
	Density (kg/m^3)	1.293
	Viscosity (Ns/m^2)	1.94E-07

We assume the surrounding gas is steady at the initial and the droplet accelerates very fast and its velocity reaches 100m/s. Before it impacts on the substrate surface, the drag force generated by the surrounding air will change its shape. During droplet spreading, after impacting with a flat substrate, free interface between the droplet and the surround air will deform continuously. A thin air gap may be trapped between the droplet and substrate. The important parameters may influence the in-flight deformation and spreading history including the particle size, morphology, velocity, material properties, and the substrate surface characteristics.

The deformation of the particle is shown in Figure 3.6(a) ~ (e). During in flight, when the morphology of the particle changes, the melt flow inside the particle is also changed, as shown in Figure 3.7. In Figure 3.6(a), there isn't so much change on the shape of the droplet, but in Figure 3.6(b) it is noticed that the air shear stress acted on the droplet surface will deform the spherical shape into a bean liked shape. Figure 3.6(c) shows that the droplet shape changes continuously when it's very close to the substrate surface. At this temperature, air pressure between droplet and substrate starts to build up. After impact, the shape of the particle is determined by the interaction between the droplet and the substrate. In this paper, we assume the droplet keep in the liquid phase and substrate surface is flat. From results, we can observe that the shape of the droplet is not a perfect spherical due to air friction. It will definitely influence the spreading behavior and the final shape of the splat.

Figure 3.7 shows the fluid field for the surrounding air and liquid flow inside the particle, which will help us understand the shape change for droplet in-flight. The melt flow in the droplet will change its shape, which will further change the drag force acted on the droplet by the surrounding gas. It will therefore influence the acceleration and heating processes. The melt flow inside the droplet will help us understand heat and mass transfer in the droplet, and it is essential to establish the relationship between in flight particle characteristics and coating properties.

Densed Spherical Particle at low Viscosity $\sigma = 0.01N/m^2$

For the particles of the same size, D=60 μm, and velocity V=100m/s but at different surface tensions numerical simulations are performed and results are shown in Figure 3.8~Error! Reference source not found.. When the particle with smaller surface tension, at the same in-flight we observed more free surface deformation, comparing Figure 3.6 and Figure 3.8, but the particle with a larger surface tension will deform less. From the results shown in Figure 3.6 and Figure 3.8 and **Error! Reference source not found.**, we can see at the beginning of in-flight, surface tension slightly influences the particle shape. At time t=0.4, the particles with different surface tensions have almost the same morphology. But the difference is noticed before the particle impacts on the substrate at time t=0.6. The bigger surface tension is, the smaller free surface deformation observes.

As we noticed in Figure 3.6 and Figure 3.8 at time t=1.0 when the spreading almost finished, there is a small gap between the droplet bottom and the substrate surface. The air entrapped between the droplet and substrate is observed. Air trapped under an impacting droplet is observed numerically and experimentally before. When the droplet comes closer to the substrate, the air gap between surfaces is compressed and the air pressure between droplet and substrate starts to build up, when the air pressure is large than the pressure inside the droplet at the bottom, the increased pressure in the air will create a dimple in the liquid surface and become a bubble in some case. If the momentum of the droplet is large, several voids or air pockets will be trapped, as shown in Figure 3.6 and Figure 3.8. This phenomenon is confirmed by the experimental study.

If the substrate wets the droplets, it will be difficult for air to be trapped. The air trapping is related to surface tension, droplet velocity, wettability, roughness and surface adsorbates. Air pressure accumulating and air escape time are the most important

parameters. In some cases, air trapping may cause a single bubble inside the molten droplet; some cases, various pores will be trapped at the bottom of the splat. The contact areas at the bottom of the splat indicate the adhesion strength; the existing pores will result in the poor contact and weak adhesion.

The particle material used in spraying is very different with a wide range of surface tension, particle velocity, and temperature, which all plays the important roles on the particle in-flight deformation and spreading. Also particle shape and porosity will affect the coating properties.

3.4.3 Hollowed Spherical Particle

Particles with different morphologies, especially, hollow particles, are used in industry, for example, YSZ hollow particles have been used for thermal barrier coating and the produced coatings have a lower thermal conductivity comparing with the densed particles. Little attention was paid to the particle impact other than the densed one. It will be different for the particle in-flight deformation and spreading; we will study the hollowed particle deformation behavior using simulation and find the difference between the densed particles and hollowed ones.

For the hollowed particles, all the input data we used are the same as solid ones expect there is a spherical hole inside; the outer diameter of the particle is $60\,\mu m$. We choose the thickness of the shell is 50% of the outer radius size as the baseline case for the hollowed particle simulation, which means that the inner diameter of the particle is $30\,\mu m$.

When the hollowed droplet is flying in the surrounding gas, at the very beginning (Figure 3.9a, t=0.2), wavy surface was developed, which is different from the densed particle (Figure 3.6 a), within the droplet, the hollow pore changes slightly. When the particle is flying further downward, shown in Figure 3.9 (b), the hole inside the particle is deformed. The deformed void moves against the flying direction and eventually, it moves to the surface and finally was released from the particle (as shown in Figure 3.9d, t=0.8).

3.5 Conclusions

A numerical model based on the level set method is adopted to simulate the droplet movement during in-flight and spreading after impact. The level set function is used to track the deformation of the droplet free surface. The capability of the model on efficiently modeling the droplet deformation and oscillation are demonstrated, and the model is used to study the melt flow inside the droplet, and deformation of the droplet. The in-flight deformation of hollowed particle and the spreading of droplet formed by hollowed particles are simulated for the first time. Numerical results show that the droplet shape is dependent of the air friction. Also air entrapment may be observed between the droplet and substrate. The role of surrounding air is important. Unfortunately, most study in the literature has neglected the surrounding gas.

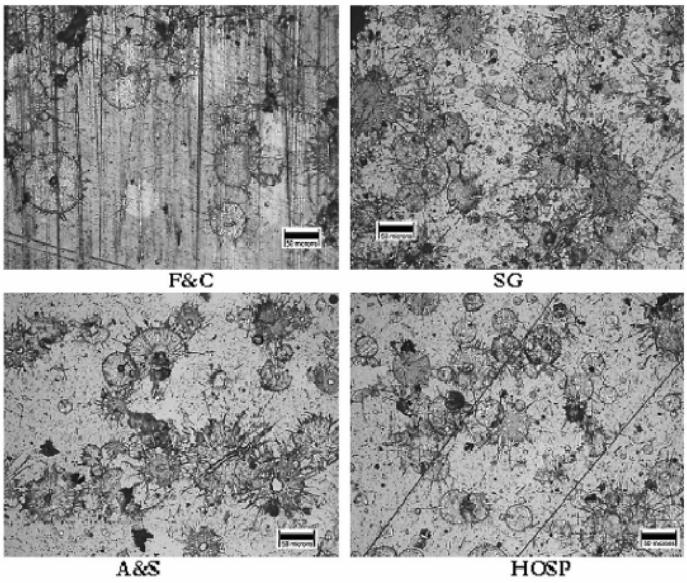

Figure 3.1 Single splat morphologies (50 μm scale-bar shown) obtained by using different particle morphologies

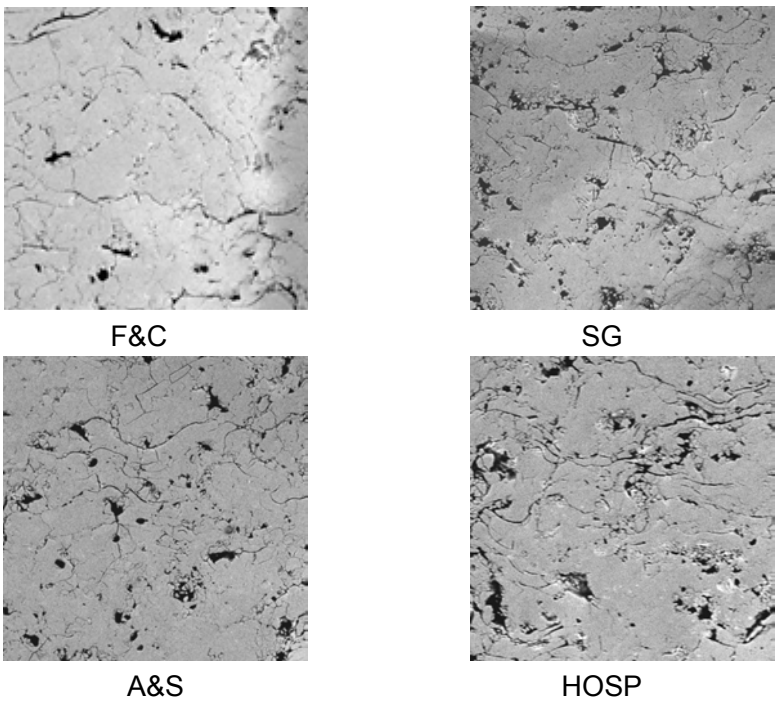

Figure 3.2 PSZ coating microstructures obtained by using different particle morphologies

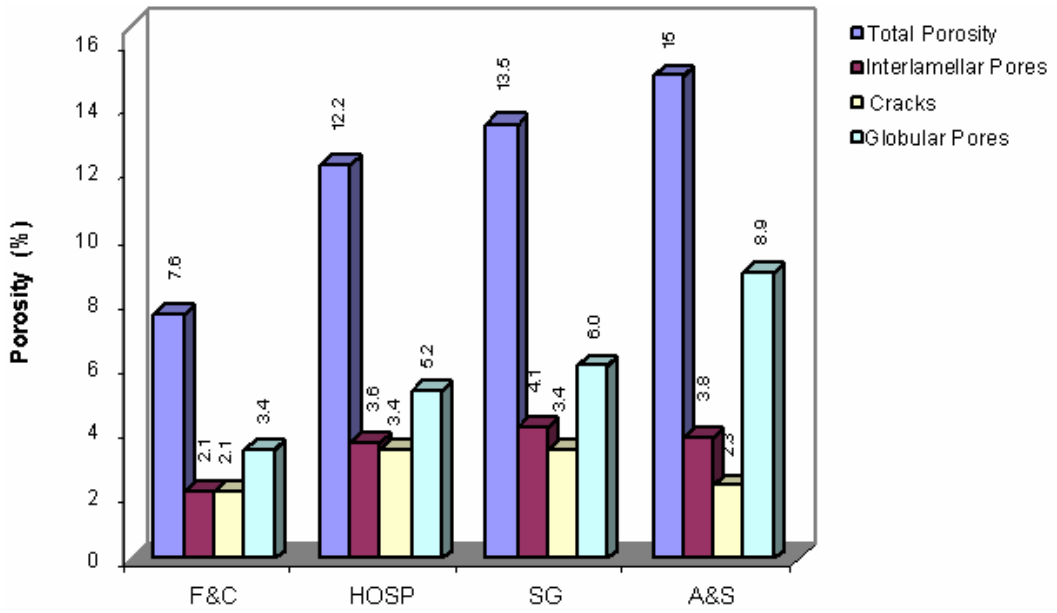

Figure 3.3 Quantitative separation of total porosity into three void systems using SANS

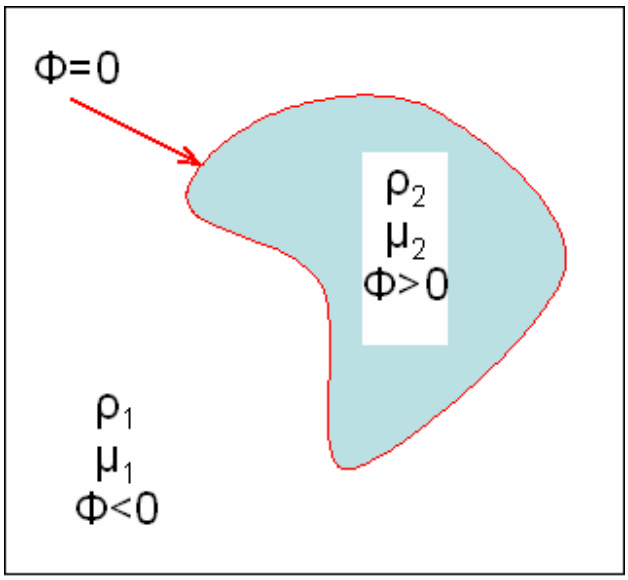

Figure 3.4 Definition of level set function

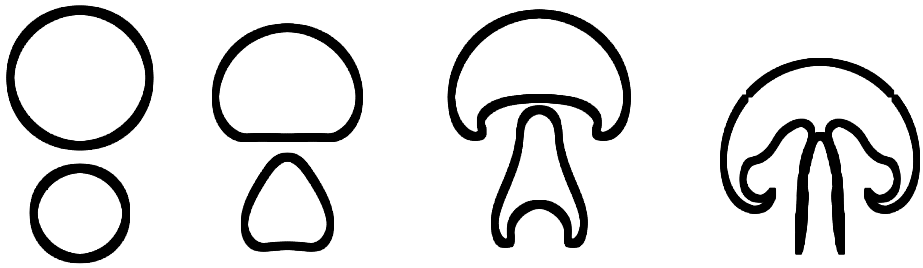

(a) t = 0 (b) t = 0.2 (c) t = 0.3 (d) t = 0.5

Figure 3.5 Second order ENO approximation for two bubbles with the same density, surface tension $\sigma = 0.005$, and different viscosity $\mu_1 = 0.0005$, $\mu_2 = \mu_1 / 2$ for t=0, 0.2, 0.3 and 0.5.

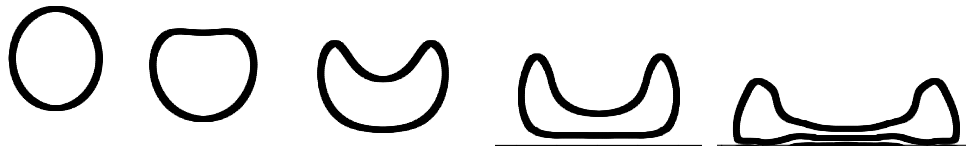

(a) t=0.2 (b) t=0.4 (c) t=0.6 (d) t=0.8 (e) t=1.0

Figure 3.6 In-flight deformation and droplet spreading with D=60 μm at different time t=0.2, 0.4, 0.6, 0.8 and 1.0, $\sigma = 0.3N/m^2$.

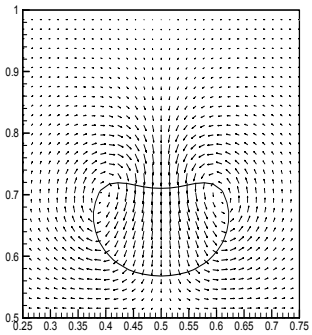

Figure 3.7 Inside flow of the particle/droplet

(a) t=0.4 (b)t=0.6 (c) t=0.8 (d) t=1.0

Figure 3.8 In-flight deformation and droplet spreading when $\sigma = 0.01N/m^2$.

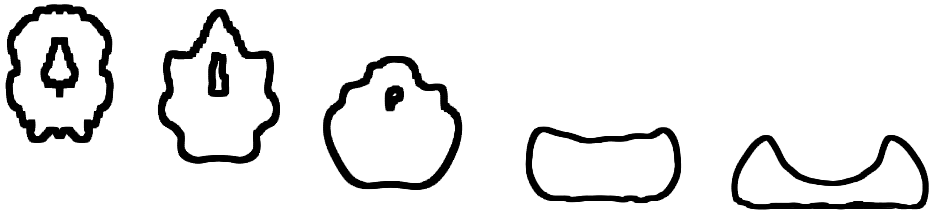

(a) t=0.2 (b)t=0.4 (c) t=0.6 (d) t=0.8 (e) t=1.0

Figure 3.9 Deformation behavior of in-flight and spreading of hollowed particle with D_{out}=60 μm, Din=30 μm, $\sigma = 0.30 N/m^2$

Chapter 4 Modeling of Substrate Melting

4.1 Introduction

Melting and re-solidification of the substrate plays an important role in thermal spray coating. It may improve bonding between the coating and the substrate but in some occasions it could damage the substrate. It is important to know the mechanism of substrate melting and its influence on the coating properties. A good understanding of this phenomenon will help us achieve better bonding.

In this chapter, a numerical model is developed to investigate the solidification of the droplet, and melting and re-solidification of the substrate. The solidification interface movement is obtained by applying a rapid solidification model on the solid/melt interface. Numerical simulations have been used to study the influence of materials and temperatures of the splat and substrate on substrate melting and re-solidification. A dimensionless parameter, temperature factor, has been proposed from analysis and can be used as an indicator whether substrate melting will occur for a certain combination of the droplet and substrate, and this parameter can be correlated with the maximum melting depth of the substrate. The possibility of heating up the substrate by plasma flame, together with a temperature-control device attached at the backside of the substrate to

achieve substrate melting was studied. The substrate front surface temperature can be controlled at a sufficient high temperature. With additional heating from superheated molten droplets and the latent heat of droplet solidification, a thin layer of the substrate can be obtained. Particle melting status, particle velocity, particle surface temperature, and controlled substrate backside temperature are important for substrate melting. It is therefore possible to make epitaxial splat deposition, and broader new applications will be possible to find.

4.2 Numerical Model of Substrate Melting and Re-Solidification

Since the splat thickness is much smaller than the splat diameter, one-dimensional heat conduction analysis is a good assumption to study melting and re-solidification processes. In the present study, the interface temperature is allowed to deviate from the equilibrium temperature and a linear kinetics relation is used to describe rapid solidification. The interfacial heat transfer coefficient is introduced at the interface between the splat and substrate to quantify the imperfect thermal contact. The phase change can take place at two solid/liquid interfaces: solidification in the splat and melting/re-solidification in the substrate.

The problem can be treated as a one-dimensional heat conduction problem with phase change taking place at two solid/liquid fronts. A molybdenum droplet impinging

on stainless steel substrate is considered as the baseline case. The governing equation can be expressed as:

$$\rho_j C_{pj} \frac{\partial T_j}{\partial t} = \frac{\partial}{\partial y}\left(k_j \frac{\partial T_j}{\partial y} \right) \tag{4-1}$$

where the subscript *j* stands for either solid (S) or liquid (L) phase in either splat or substrate, *T* is the temperature, *t* is the time, *y* is the vertical coordinate normal to the substrate surface, and ρ, *Cp*, and *k* are density, capacity, and heat conductivity, respectively. *y=0* is set at the initial substrate/splat interface.

The thermal contact resistance between the splat and substrate can be quantified by interfacial heat transfer coefficient *h*,

$$+k \frac{\partial T}{\partial y} = h(T_{SB} - T_{ST}) \tag{4-2}$$

where: T_{SB} and T_{ST} are the bottom surface temperature of the splat and top surface temperature of the substrate, respectively. The contact resistance is a complex function of the processing conditions. Quantitative information has been provided in the open literature (Clyne 1984; Wang, Wang et al. 1998; Wang and Matthys 2002). The substrate temperature far away from the splat is assumed to remain at the initial substrate temperature:

$$T\Big|_{y=-\infty} = T_0 \tag{4-3}$$

The top surface of the splat is assumed to be adiabatic:

$$\frac{\partial T}{\partial y}\Big|_{y=b} = 0 \tag{4-4}$$

where: b is the thickness of the splat. Initially, the splat and substrate are assumed to be at uniform temperatures equal to the initial splat temperature (T_P) and initial substrate temperature (T_0), respectively. Thermal radiation at the liquid surface is neglected, because heat transfer by radiation is found to be much smaller than conductive heat transfer from the substrate.

In thermal spray processes, rapid cooling may result in significant melt undercooling. The interface velocity and temperature are unknown. In addition to energy balance condition, a kinetic relationship, which correlates the interface velocity and temperature, can be used. A linear relationship is a good approximation if the deviation of the interface temperature from the equilibrium melting temperature is moderate (Clyne 1984; Wang and Mattys 1996) :

$$V_i = \mu_k (T_m - T_i) \tag{4-5}$$

where: μ_k is the linear kinetics coefficient. It should be noted that although the linear kinetics equation was derived from the crystallization kinetics, it could also be applied as a first approximation to the melting process. The energy balance condition at the solid/liquid interface can be written for both splat and substrate as:

$$\rho_L L \frac{dS}{dt} = k_s \frac{\partial T_s}{\partial y}\Big|_i - k_L \frac{\partial T_L}{\partial y}\Big|_i \tag{4-6}$$

where L is the latent heat of fusion, S is the solidification thickness, and ρ_L is the density of the melt. The subscripts S and L represent solid and liquid phases, respectively. The subscript ***i*** indicates that the gradients are evaluated at the solid-liquid interface.

The nucleation is assumed to take place heterogeneously on the substrate surface at a nucleation temperature T_N, which is lower than the equilibrium melting temperature

T_M. The subsequent splat solidification may include undercooling. The melting of the substrate is assumed to occur when top surface temperature of the substrate reaches its equilibrium melting temperature, because the nucleation kinetic barrier for melting of a solid is small. Re-solidification of the melted substrate will begin when the heat flux from the solid/liquid interface into the solid substrate is larger than that from the melt into the interface. No nucleation model is necessary because the melt is already in contact with its own crystalline phase.

4.3 Numerical simulations

The governing equations describe heat transfer and solidification kinetics in both splat and substrate. During solidification, the interface position is advanced explicitly using the kinetics relationship; whereas the new interface temperature is calculated implicitly using the energy balance condition. An implicit control volume integral method with moving interface is employed (Wang, Prasad et al. 1997). A very fine time step of 10^{-4} μs is used at the earlier transient stage when the droplet has been deposited on the substrate. At the later stage, a larger time step is used to reflect the fact that the heat transfer process has been dramatically slowed down. When the droplet impacts on a substrate, the energy equation along with interface conditions is solved in the vicinity of the interface using 600 grids on each side to ensure that grid independent results are obtained.

4.4 Results and discussion

4.4.1 Substrate melting

Metallurgical bond between the impinging particle and the substrate surface due to substrate melting contributes significantly to coating adhesion strength. A good understanding of this phenomenon is essential to determine the proper bond coat to use as well as to avoid substrate damage. Molybdenum powder with a mean size of 28μm from Osram Sylvania has been plasma sprayed on mirror polished stainless steel (type 304), brass (type 260) and aluminum (type 5052) substrates. A Miller SG-100 torch is used for spraying. Splats are obtained by rapidly moving the torch across the substrate surfaces. Typical flower-like shaped splats are observed in each case, which indicates the same splats forming mechanism. Splat samples were also impregnated with epoxy and then cut and polished. The typical cross-sections of splats can be provided. It is evidenced in cross-section views that the substrates were melted and interacted with the spreading droplet.

The maximum melting depth is measured by means of scanning white light interferometry (Zygo New Viewer 200). About 20 splats are measured in each substrate. Figure 4.1 shows the top and cross-sectional views of the splat morphology during substrate melting for Mo on stainless steel, brass (70%Cu) and aluminum. Intermetallic

compounds were detected from the transmission electron microscopic (TEM) image between the splat and substrate and adhesion test proved that this layer is necessary to improve the bond between the sprayed material and the substrate.

Figure 4.2 shows the schematic diagram of the splat solidification and substrate melting process. To study the interaction between the splat solidification and substrate melting, both phase-change interfaces have to be tracked which is very difficult to perform two- or three-dimensional simulations. Numerical simulations have been conducted to investigate the melting and re-solidification of a Molybdenum droplet impacting on above three substrates at the same operating conditions. Thickness of the molybdenum splat is assumed to be $2\mu m$. Corresponding thermal properties can be found in Table 2.

Table 2 Thermal properties used in the calculations

	Molybdenum	Steel	Brass	Aluminum
T_m (K)	2883	1788	1188	933.6
h_f(J/kg)	3.71×105	2.72×105	0.13×105	3.97×105
k_l(W/m-k)	46	26	50	105
k_s(W/m-k)	84	28	111	210
C_{pl}(J/kg-k)	570	866.67	380	1080
C_{ps}(J/kg-k)	339	690.82	380	1180
ρ_l(kg/m^3)	9350	7700	8530	2390
ρ_s(kg/m^3)	10220	7850	8530	2550
α_l(m^2/s)	0.86×10-5	0.39×10-5	0.86×10-5	4.1×10-5
α_s(m^2/s)	2.43×10-5	0.52×10-5	3.42×10-5	7.0×10-5
μ_k(m/s-k)	0.26	0.01	1	1.74

4.4.2 Droplet solidification and substrate melting

Substrate melting may take place when a molten metal droplet, which has a high melting point, impacts on a substrate. If substrate melting happens, two moving solid/liquid interfaces may exist simultaneously: solidification interface in the splat and melting/re-solidification interface in the substrate. Zhang et al. (Zhang, Wang et al. 2001) showed that substrate melting would occur when a molybdenum droplet impacts on steel substrate. Since the melting points of brass and aluminum are lower than that of stainless steel, it is expected that substrate melting will also occur in both substrates. Since the melting and re-solidification of the substrate is crucial for the bonding of the coatings. We will pay special attentions on thermal histories of substrate melting and re-solidification, different time scales and maximum melting depths. Figure 4.3 shows that the temperature history of the substrate and splat as a function of time. It is assumed that the interfacial heat transfer coefficient is unchanged during the entire process. As we can be seen in Figure 4.4, the splat solidification is completed within 0.5μs if interfacial heat transfer between the thin splat and substrate is high e.g. thermal contact between two materials is very good.

As the splat solidifies, substrate temperature increases, as shown in Figure 4.3. The top surface temperature of the substrate reaches its melting temperature before the splat is completely solidified. The substrate will melt continuously for a period of time, and begin to re-solidify after latent heat from the splat is no longer transferred into the substrate to sustain melting. The interface velocities in the splat and substrate as a function of time are shown in Figure 4.5.

4.4.3 Critical conditions for substrate melting

Figure 4.6(a) shows the solid/liquid interface locations in the substrate as a function of time for five different splat temperatures from superheating to undercooling. After a delay to heat the substrate from initial temperature to its melting temperature, the substrate starts to melt and the solidification interface moves deeper into the substrate. The higher the droplet temperature is, the earlier the substrate melting begins; the faster the solid/liquid interface; the deeper the substrate will melt; and the longer the melting will last. After the maximum melting depth is reached, the melt will re-solidify. The interface locations in the substrate with different initial substrate temperatures are shown in Figure 4.6(b). For the cases shown here, the higher the substrate initial temperature is, the earlier the substrate melting begins; the later re-solidification finishes; and the deeper the substrate melts. Notes that the initial substrate temperature has a significant influence on the splat morphologies. A splashed splat may be obtained if the initial temperature of the substrate is low. In this paper, a disk-like splat is assumed for all cases. Figure 4.7 shows the effect of the interfacial heat transfer coefficient on the substrate melting. It can be seen that the increase of interfacial heat transfer coefficient results in more substrate melting. The substrate surface temperature increases much faster if interfacial heat transfer coefficient is larger or thermal contact is better. When the solidification interface reaches the top substrate of the substrate, re-solidification of the substrate is completed and both the substrate and splat will be cooled together as solids. In reality, the intermetallic alloys will be formed between the splat and substrate. The thickness of the

intermetallic alloy layer is a function of fluid field and mass transport. In this paper, convection, mixing, and intermetallic alloy formation have been neglected.

4.4.4 Substrate material effects

Figure 4.8 (a) shows the transient behavior of the re-melting process for molybdenum splats on stainless steel, brass and aluminum substrates. The initial splat temperature is $3200^{o}C$ or $3473K$ and initial temperature of the substrate is $25^{o}C$ or $298K$. The properties of the splat and substrate are listed in Table 1. In all three cases, both simulations and experiments show that the substrate melting happens. The melting interface moves downward until it reaches the maximum melting depth, the substrate re-solidification process will then start. Figure 4.8 (b) shows the temperature history on the top surface of the substrate for three substrates. The top surface temperature of stainless steel is the highest and temperature of aluminum is the lowest. Figure 4.8 shows the simulation results of the substrate melting time, re-solidification starting time, and re-solidification completed time for three different substrates. For stainless steel, brass and aluminum substrates, after the droplets impinging on the substrate, the substrate re-melting begins at 0.09, 0.03 and 0.02 μs, respectively; the re-solidification begins at 0.50, 0.65 and 0.75μs, respectively; and ends at 0.89, 1.43 and 2.08μs, respectively. The surface temperature history, melting starting time, re-solidification starting and end times are all related to thermal properties of the materials. For aluminum, since its thermal conductivity is the largest and the melting temperature is the lowest, the time when substrate reaches its melting temperature will be the shortest.

4.4.5 Maximum melting depth

If the substrate starts to melt, the maximum melting depth achieved in the substrate is an important parameter for the bonding quality. The maximum melting depth may affect the microstructure of coatings. On one hand, a large melting depth may be helpful to ensure the appropriate bonding between the coatings and substrate. On the other hand, it may damage the microstructure of the substrate. It may be needed to achieve an appropriate compromise between the conflicting requirements. Figure 4.6(a-b) and Figure 4.7 show that the maximum melting depth under various conditions for molybdenum splats on different substrates. It can be seen that the splat temperature, substrate material, initial substrate temperature, and interfacial heat transfer coefficient all play important roles on the maximum depth of the substrate melting. Increase the initial temperature of the splat and substrate will result in increase in the maximum melting depth. In addition, it can also be seen that for a given splat temperature and initial substrate temperature, increase in interfacial heat transfer coefficient will greatly increase the maximum melting depth. Figure 4.8shows that the maximum melting depths for three different substrates - stainless steel, brass and aluminum. Figure 4.9 shows the comparison between experiments and simulations for the maximum melting depth. It seems that the simulation results have under-predicted the maximum melting depth. One of reasons may be that convective heat transfer due to the molten liquid movement in the spreading process is important, which have been neglected in our model. The enhanced heat transfer by convective will melt the substrate more.

4.4.6 Dimensionless parameter for substrate melting

To obtain analytical results of the substrate melting, the thermal history of the process can be simplified as a uniform layer of liquid at initial temperature T_p suddenly brought into contact with a substrate at initial temperature T_0. The problem under consideration is a one-dimensional heat transfer problem. Assuming that the splat and substrate is semi-infinite substances and contact between the splat and substrate is perfect, e.g., contact thermal resistance is negligible, and temperature distributions in the solid and liquid phases will satisfy the heat diffusion equation separately.

$$\frac{\partial T_i}{\partial t} = \alpha \frac{\partial T_i^2}{\partial y^2} \tag{4-7}$$

where thermal diffusivity $\alpha = k_i / \rho_i C_{pi}$, the subscript i stands for either splat (*sp*) or substrate (*sub*), and k, ρ, C_p are heat conductivity, density and specific heat, respectively. Since perfect contact between splat and substrate is assumed, the top surface temperature of the substrate and the bottom surface temperature of the splat should be the same, and also the heat fluxes should be continued,

$$-k_{sp} \left. \frac{\partial T_{sp}}{\partial y} \right|_{y=0} = -k_{sub} \left. \frac{\partial T_{sub}}{\partial y} \right|_{y=0} \tag{4-8}$$

To satisfy the above two conditions, the interface temperature between the substrate and splat can be approximated as follows (Mills, 1999)

$$\frac{T_0 - T_i}{T_i - T_p} = \left(\frac{k_{sp} \rho_{sp} C_{psp}}{k_{sub} \rho_{sub} C_{psub}} \right)^{0.5} \tag{4-9}$$

It can be rewritten as

$$T_i = \frac{T_0 + \beta T_P}{1+\beta} \tag{4-10}$$

where $\beta = \left(k_{sp}\rho_{sp}C_{psp}/k_{sub}\rho_{sub}C_{psub}\right)^{0.5}$, T_0 is the initial substrate temperature in K, and T_p is the initial splat temperature in K. If Ti is greater than the melting temperature of the substrate, the substrate melting will occur. We can design the following parameter, called temperature factor, as

$$\Delta = \left(T_i - T_m\right)/T_m \tag{4-11}$$

It can be used to determine the potential of the substrate melting. The calculated results are also shown in Figure 4.10. From results, the temperature factor is closely correlated with the maximum melting depth. The temperature factor defined in Equation (4-11) can therefore be used as an indicator whether a substrate melting will occur for a certain combination of the droplet and substrate.

4.4.7 Substrate temperature control system

In traditional thermal spraying, substrate is kept at a far location and substrate melting will usually not happen. If a substrate heated by the external laser, substrate melting may happen locally and adhesion of the splats is expected to be improved. However, the laser heating will only appear locally. Also the cost of the process will be dramatically increased. Here we propose to heat up the substrate by the plasma gun, e.g., we move the substrate closer to the nozzle. Together with a cooling device attached at the

backside of the substrate, it is expected that the front surface temperature of substrate can be controlled at a sufficient high temperature. With additional heating from superheated molten droplets and the latent heat of droplet solidification, a thin layer of the substrate will be melted and epitaxy growth of the splats is possible. How to control the substrate surface temperature will be investigated. Numerical models will be used to predict substrate melting, and droplet morphology.

In traditional thermal plasma spraying, the standoff distance is about 100mm. The flame is far from the substrate and substrate temperature remains low. Substrate melting will not happen unless the melting temperature of sprayed material is much higher than the substrate material. If we could achieve substrate melting for any material combination, similar to laser heat, plasma flame can be used to heat the substrate close to the melting temperature. The impact of droplet will be possible to melt the substrate and initial solidification. To control the re-melt and solidification, we can use the cool device at the backside of the substrate. The droplets will impact on the substrate with the prescribed front surface temperature and temperature gradient inside. The traditional substrate melting model is not suitable for this system since the initial substrate temperature is no longer uniform. To simplify the analysis, we assume that the previous analytical model is applicable if the initial substrate temperature is changed to the substrate surface temperature. Since we want to calculate the contact temperature, this assumption is reasonable. The design is shown in Figure 4.11. The heat flux to the substrate is contributed by the flame jet and impacting particles. The level of heat flux at the substrate will is directly related to stress developed and substrate deformation. With flame and particle temperatures from process modeling, the heat flux to the substrate can

be calculated. Comparing with substrate melting by traditional plasma spray technology, the temperature distribution before and after droplet impacting is shown in Figure 4.12.

When droplets solidified on a thin layer liquid at the top of the substrate, conditions will be similar to crystal growth. Epitaxy film growth is therefore possible. The quality of the coatings will be significantly improved. It may be possible to extend traditional plasma spray technologies into meso-scale electronics applications. In this paper, we will exam the possibility of this technology from numerical simulation.

The LAVA3D-P computational model has been developed to simulate three-dimensional, compressible, turbulent reacting flow and model particle's acceleration, heating, melting and oxidation within the flame jet (Xiong, 2004). In addition, it can handle multiple (several thousands or more) particles in-flight simultaneously and predict the distributions of particles velocity, temperature. From LAVA3D-P model, we can obtain flame temperature T_f and particle temperature T_p at different standoff distances for ZrO_2 particle shown in Figure 4.13.

Using the substrate cooling from the backside, we can have a cold substrate backside temperature at T_0. The substrate front face temperature T_{ss} can easily derived by the fact that the summary of heat flux of convection with the flame temperature T_f and the heat flux of radiation with environment (when the substrate is heated by flame, it can't be ignored) is equal to the heat flux of conduction inside the substrate:

$$h(T_f - T_{ss}) + h_{rad}(T_{ss} - T_\infty) = k_{sub}(T_{ss} - T_0)/b \qquad \textbf{(4-12)}$$

Where: h is the heat transfer coefficient, its value is set to 3000 W/m^{2}K (Xiong 2004); b is the thickness of the substrate, we use 5mm in our simulation; $h_{rad} = \varepsilon\sigma\overline{T}_{ss}^{\ 3}$; emissivity ε=0.5; Stefan's constant σ=5.67x10^{-8}W/m^{2}K; $\overline{T}_{ss}$=1650K, and T_∞=300K. We have:

$$T_{ss} = (T_f + T_0 \frac{k_{sub}}{bh} - T_\infty \frac{h_{rad}}{h}) / (1 + \frac{k_{sub}}{bh} - \frac{h_{rad}}{h}) \quad \textbf{(4-13)}$$

After droplet impacting, the temperature evolution is similar as traditional substrate melting. The contact temperature between droplet and substrate T_j can be controlled to slightly higher or lower than the substrate melting temperature T_m, and its value can be derived by:

$$T_j = (T_{ss} + \beta T_p) / (1 + \beta) \quad \textbf{(4-14)}$$

where: $\beta = \left(k_{sp}\rho_{sp}C_{psp} / k_{sub}\rho_{sub}C_{psub}\right)^{0.5}$. If T_j is greater than the equilibrium melting temperature of the substrate, substrate will be melted. We use the temperature factor similar as in traditional substrate melting by using T_j as the interface temperature instead of T_i :

$$\Delta = \left(T_j - T_m\right) / T_m \quad \textbf{(4-15)}$$

Figure 4.14 shows that the substrate melting factor as a function of substrate temperature for different splats without substrate temperature control. When the factor is larger than 0 it means substrate melting happen. From this figure we can tell that in traditional thermal spraying, substrate melting doesn't always happen: for Mo on stainless steel, there is substrate melting when the substrate is at room temperature. But for ZrO_2 on stainless steel, we haven't observed this phenomenon even with very high substrate initial temperature.

We studied ZrO_2 droplet with/without substrate temperature control. For stainless steel substrate, results for substrate surface temperature and temperature factor are showed in Figures 4.15-16. The melting temperature of stainless steel is 1788K, T_{ss} is about 250K lower than T_m at standoff distance 4cm and about 500K lower at standoff distance 6cm. T_{ss} can be controlled by the distance of the substrate location easily. T_{ss} will be increased by the superheated droplet after impacting and substrate will be melted. When we use substrate temperature control in thermal spraying, results are very different, as shown in Figure 4.16. In the calculation, we used flame temperature T_f and particle temperature T_p at different standoff distances from Figure 4.13, we set T_0=600K and obtained the temperature factor. We use the same flame and particle condition, only change T_0 to 900K and 1200K, the results for temperature factor shown in Figures 4.17-18. When the factor is larger than zero, it means that substrate melting happens. As shown in these figures, the front surface temperature of substrate can be controlled at a sufficiently high value. With additional heating from superheated molten droplets and the latent heat of droplet solidification, a thin layer of the substrate melting and directional solidification of the splats can be obtained.

Results show that substrate melting happens at a smaller standoff distance when the substrate is cooled at the backside. When the substrate backside temperature T_0 is 600K, substrate melting is obtained for spray distances around 5cm. With T_0=900K this distance change to around 6cm; the substrate will melt at spray distance of round 7cm with T_0=1200K. The higher the substrate backside temperature, the longer spray distance we need to get substrate melting.

There are several issues should be resolved before it can be used in practice. At the current system, the standoff distance is shorter. The particles may not have sufficient time to be fully melted. The second issue is stress development in the coating. The heat flux to the substrate is contributed by the flame jet and impacting particles. The level of heat flux at the substrate will is directly related to stress developed and substrate deformation. A backside temperature around 1200K is recommended for the substrate melting can be obtained at spray distance around 7cm, which gives the in-flight particles sufficient residence time to be melted and accelerated. It can be clearly seen from the process that particle melting status, particle velocity, particle surface temperature, spray distance and controlled backside substrate are important for substrate melting. The results show that proposed design is capable of controlling the substrate melting by control the spray distance and substrate backside temperature.

4.5 Conclusions

A numerical model is developed to calculate substrate melting and re-solidification when a molten droplet impacts on a substrate. This model has been used to calculate the temperature history and the solid/liquid interface location. For a given materials pair, substrate melting and re-solidification is investigated. Simulation results reveal that initial splat and substrate temperatures play important roles on the maximum melting depth of the substrate and thus on the bonding of the coatings. The results also confirm that

imperfect contact, interfacial heat transfer coefficient, will have a significant influence on substrate melting and re-solidification. Substrate melting and re-solidification also depends on thermal physical properties of the materials. From analysis, a dimensionless parameter, temperature factor, has been proposed and can be used as an indicator whether a substrate melting will occur for a certain combination of the droplet and substrate, and it can be correlated with the maximum melting depth of the substrate. A design is proposed to heat up the substrate by the plasma gun together with a cooling device attached at the backside of the substrate, by which the substrate front surface temperature can be controlled at a sufficient high temperature. With additional heating from superheated molten droplets and the latent heat of droplet solidification, a thin layer of the substrate will be melted and epitaxy growth of the splats is possible.

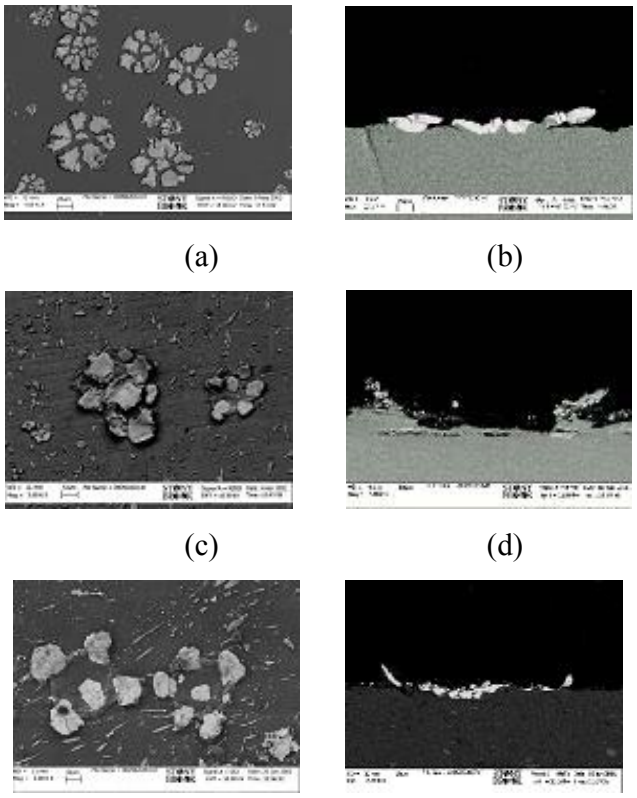

Figure 4.1 Top and cross-sectional views of the splat morphology during substrate melting for Mo on (a-b) stainless steel, (c-d) brass (70%Cu) and (e-f) aluminum

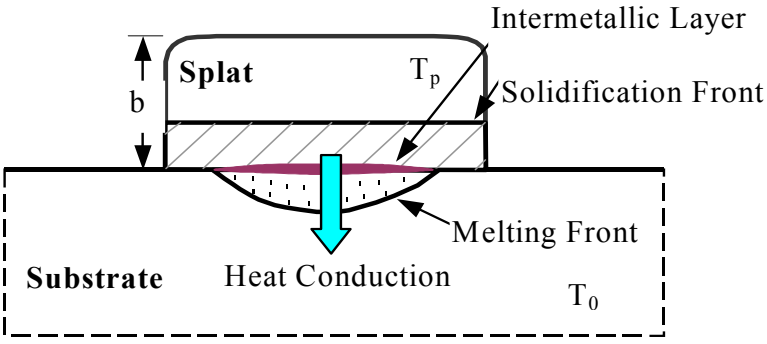

Figure 4.2 Schematic of the splat solidification and substrate melting for Mo on steel

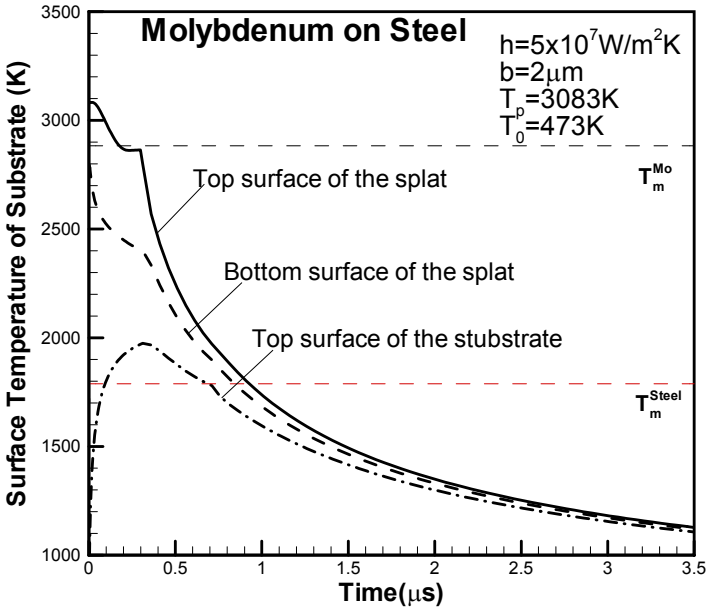

Figure 4.3 Temperature history of the splat and substrate for a molybdenum splat on steel substrate

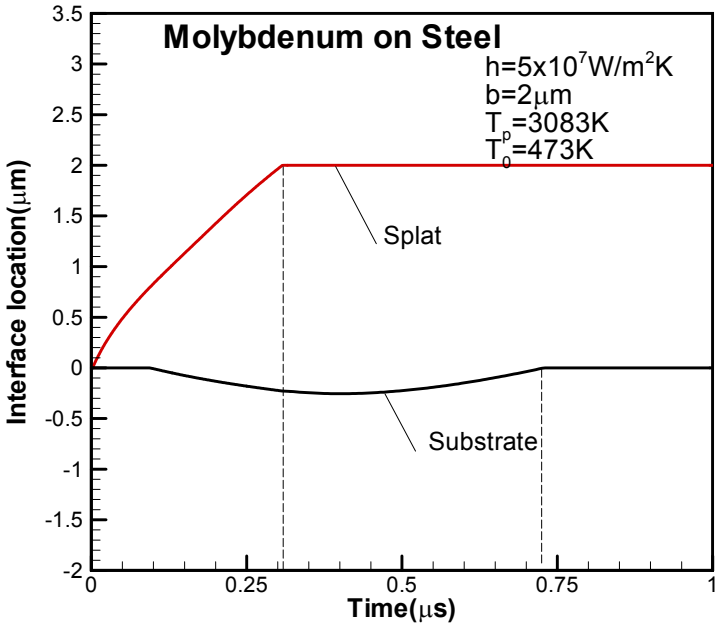

Figure 4.4 Interface locations during solidification of the splat and melting/re-solidification of the substrate

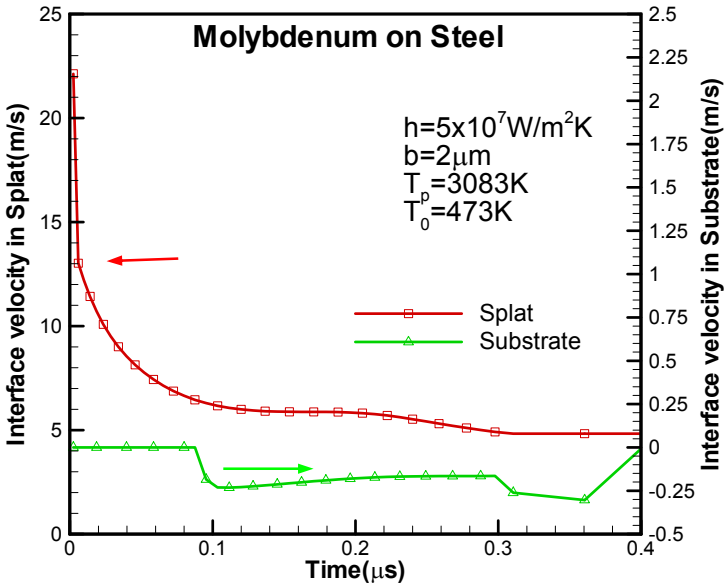

Figure 4.5 Interface velocities of the splat and substrate as a function of time

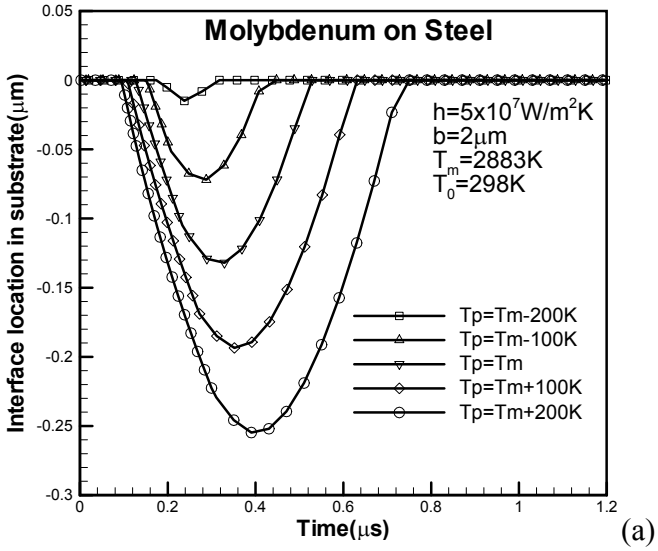

(a)

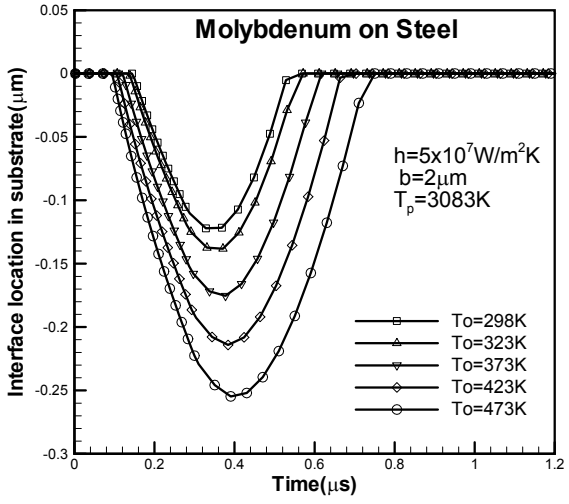

(b)

Figure 4.6 Interface locations as a function of time during the melting and re-solidification of the substrate for different (a) splat temperatures, (b) substrate temperatures

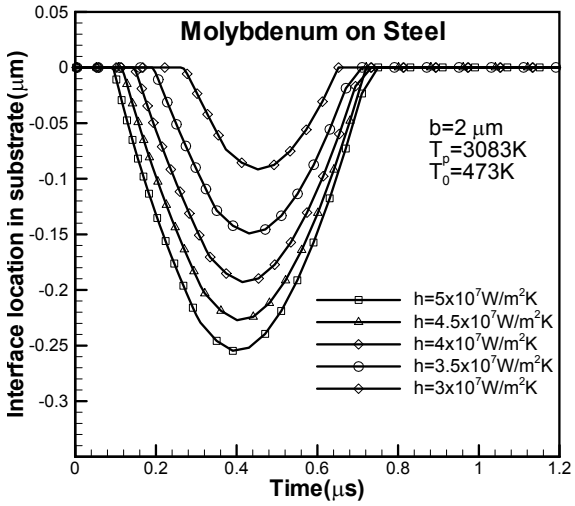

Figure 4.7 Interface locations as a function of time during the melting and re-solidification of the substrate for interfacial heat transfer coefficients

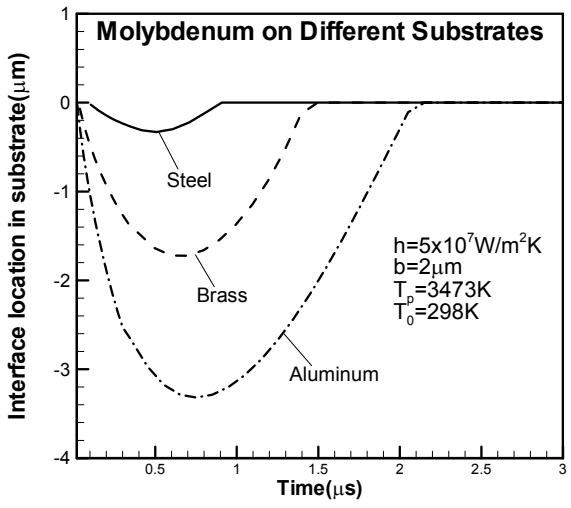

(a)

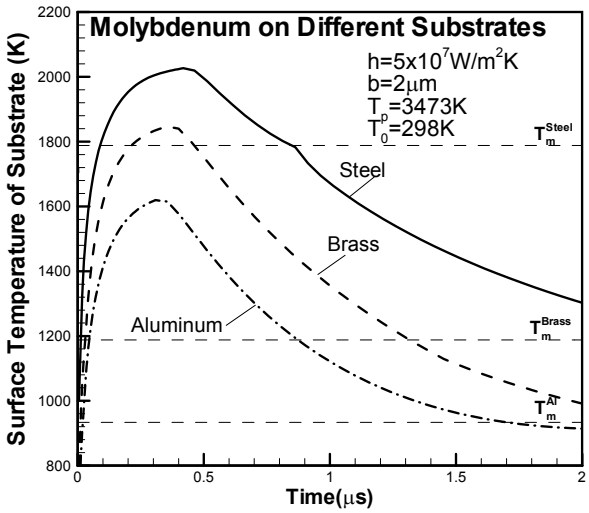

(b)

Figure 4.8 (a) Interface locations for three different substrate materials. (b) Temperature history of the top surface temperatures of the substrates

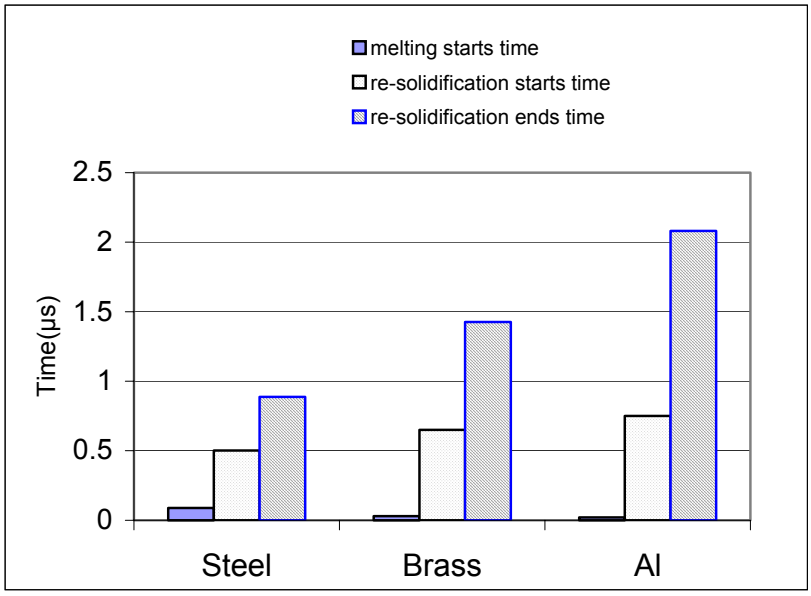

Figure 4.9 Numerical predicted time scales of the melting and re-solidification of the substrates

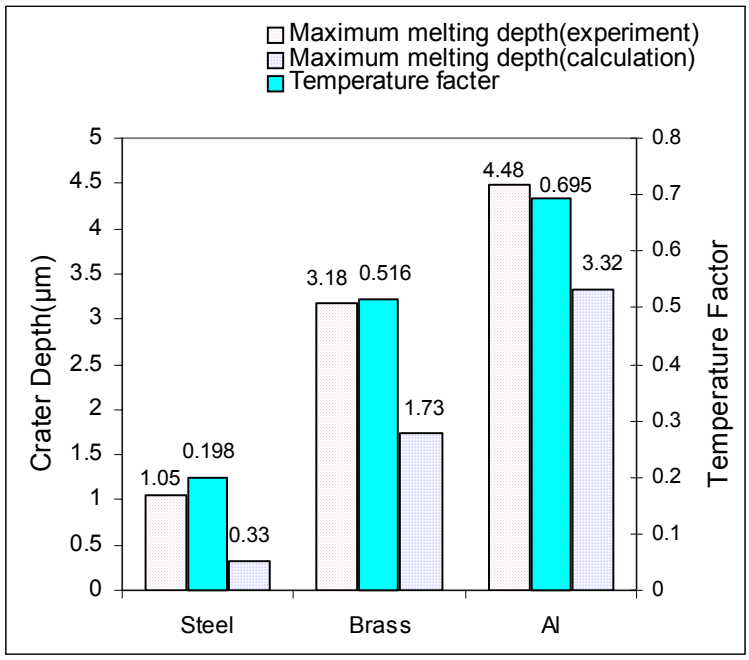

Figure 4.10 Comparison between the experimental and simulation results

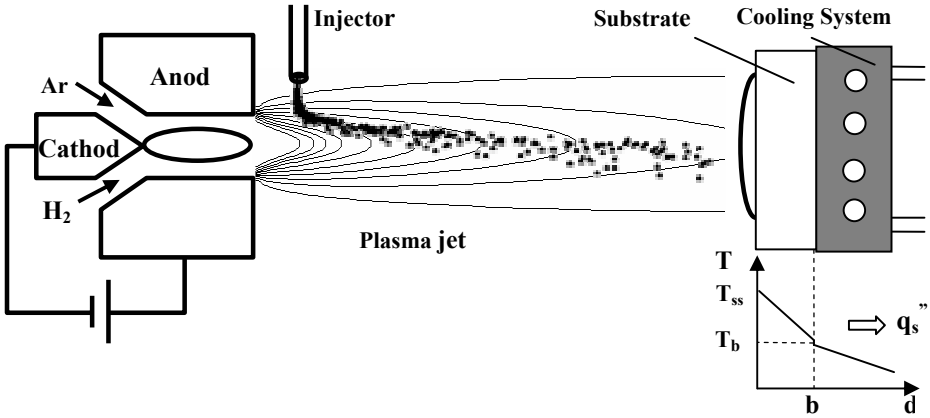

Figure 4.11 Schematic of thermal spray coating with substrate temperature control system and temperature distribution in the substrate and cooling device.

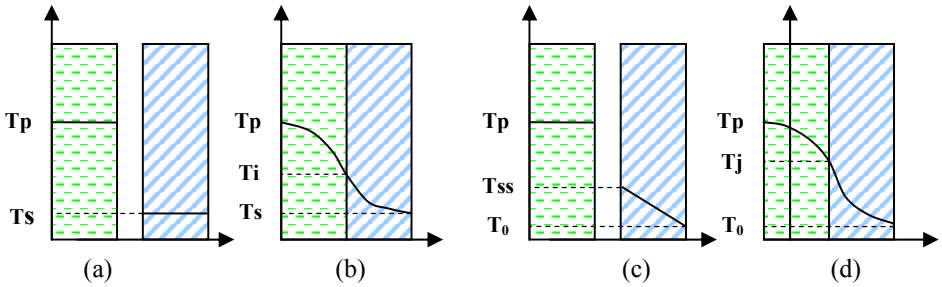

Figure 4.12 Schematic of temperature distribution inside the droplet and substrate for thermal spray without substrate temperature control device(a) Before impacting; (b) After impacting; and with the device (c) Before impacting; (d) After impacting.

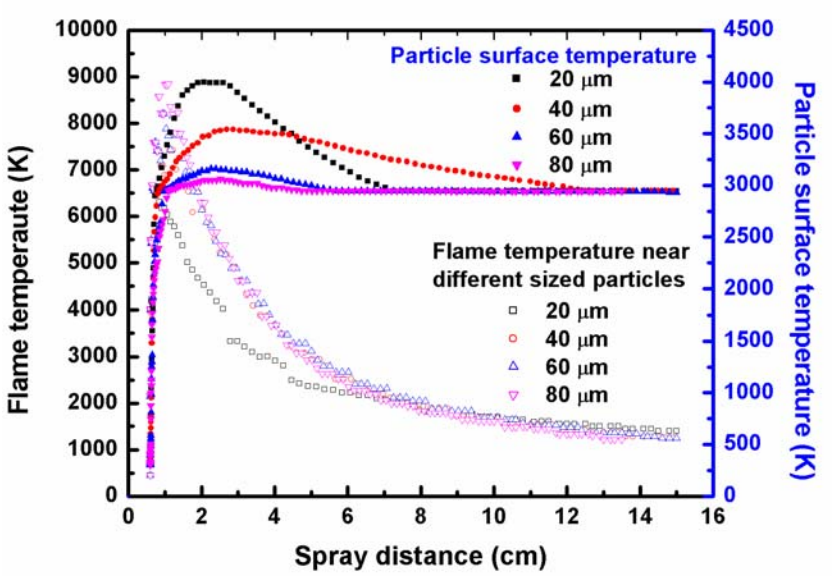

Figure 4.13 Flame and particle temperatures vs standoff distance for different particle sizes.

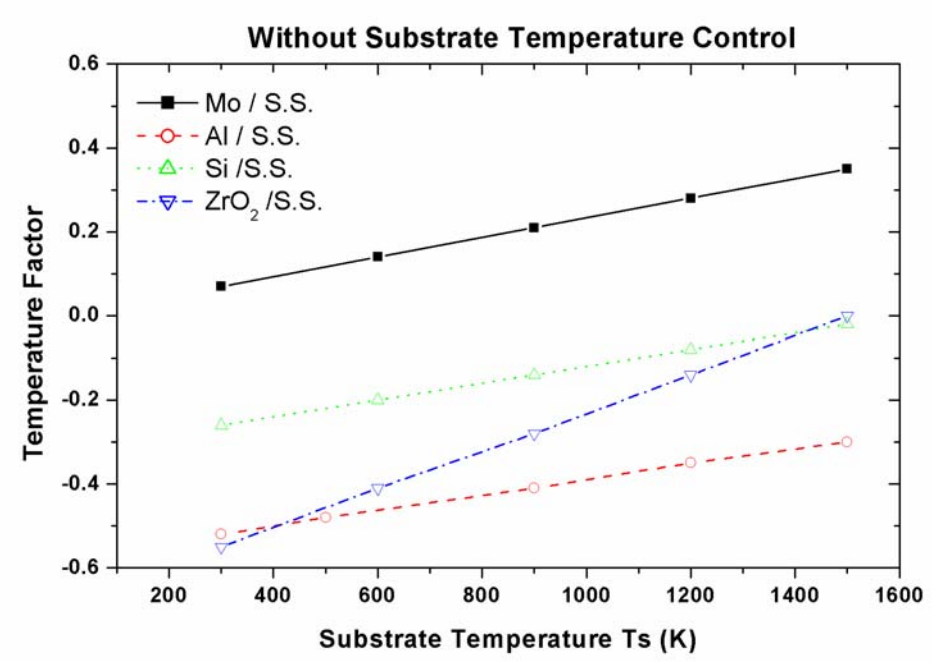

Figure 4.14 Temperature factor versus substrate temperature for different splats in tradition thermal spray technology.

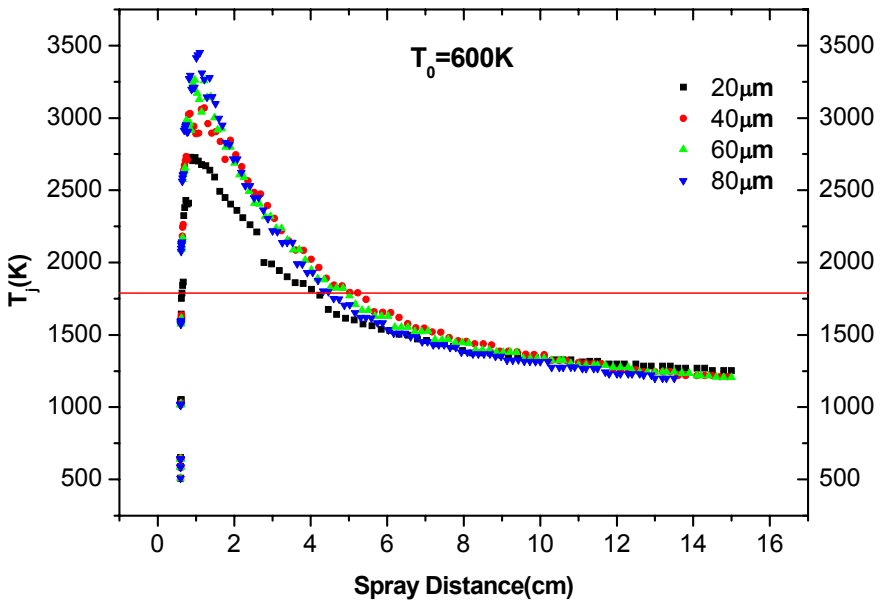

Figure 4.15 Substrate surface temperature versus standoff distance for different splats

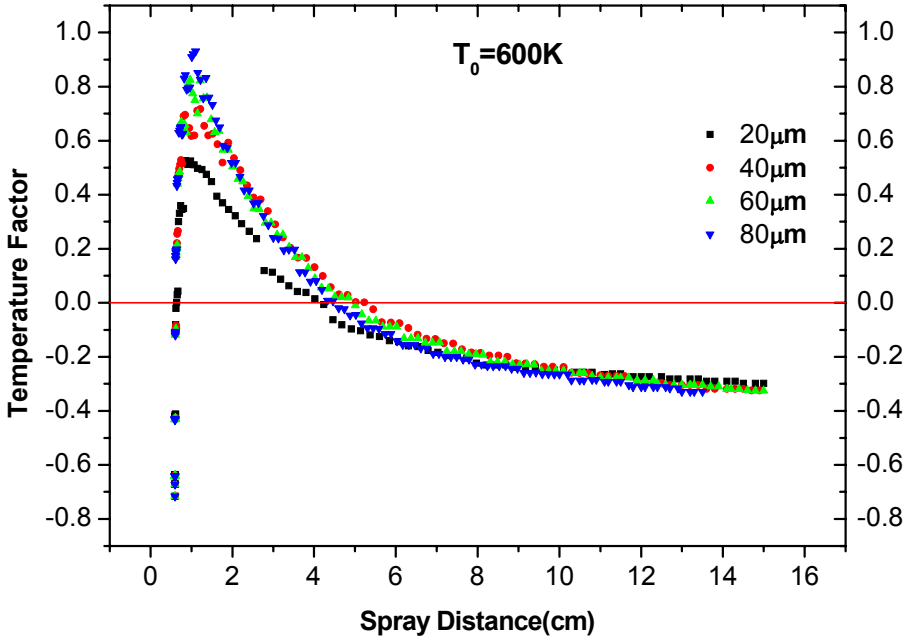

Figure 4.16 Temperature factor vs standoff distance for ZrO_2 on stainless steel with substrate temperature control system: T_0=600K.

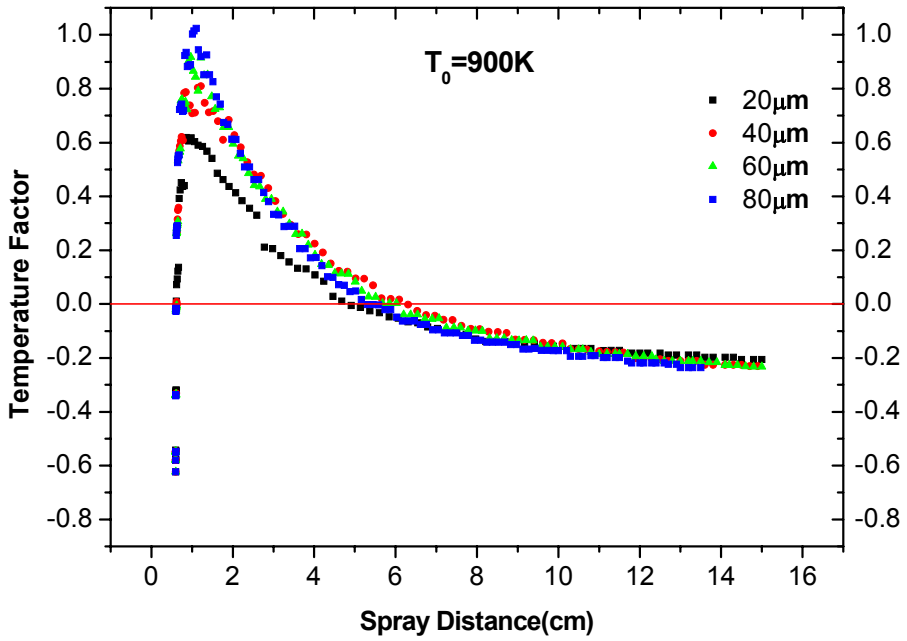

Figure 4.17 Temperature factor vs standoff distance for ZrO_2 on stainless steel with substrate temperature control system: T_0=900K.

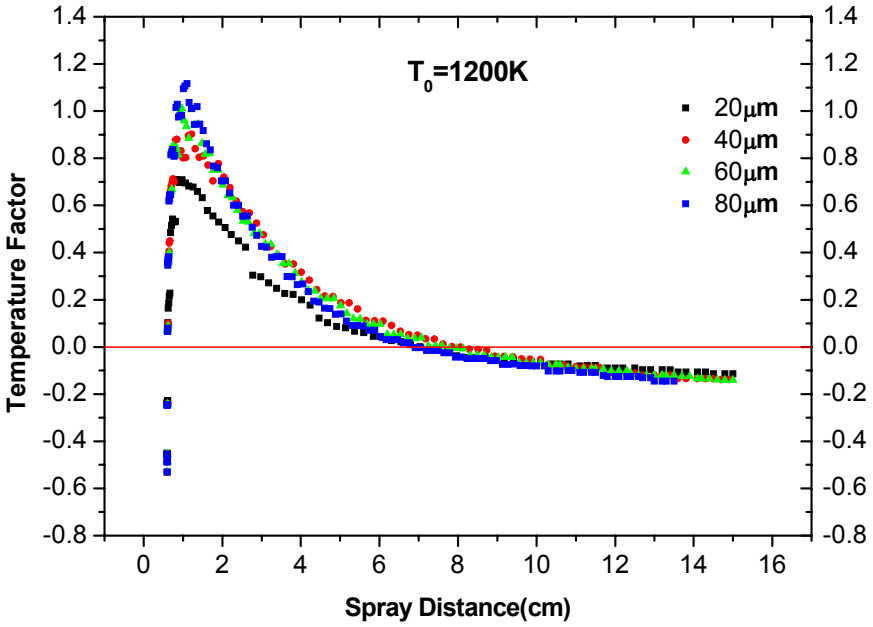

Figure 4.18 Temperature factor vs standoff distance for ZrO_2 on stainless steel with substrate temperature control system: T_0=1200K.

Chapter 5 Modeling of Coating Buildup

5.1 Introduction

The coating production by thermal spraying offers a wide range of applications. This method for production of functional coating on technical surface have been developed and optimized for more than 30 years. The coating properties depend critically on the thermal- and kinetic-energy histories of the particles entrained in the plasma flame and substrate conditions. The development of new coating systems and optimization of processing procedures is still carried out through time intensive and expensive trial and error approaches. For more effective development of coating it is necessary to reach a correlation between spray parameters and coating characteristics.

In this chapter, we use a comprehensive three-dimensional computational code (LAVA3D-P) to predict the plasma flame formation, flame and particle interaction, and particle state and trajectory. Mean values and standard deviations of particle size, velocity, and temperature, and impact position are obtained from in-flight particle simulations. These spray parameters controlled droplet characteristics together with the given substrate conditions will be used as the initial condition of splat morphology prediction and in turn as the input of the entire coating build-up process. We proposed a

set of coating build-up rules to predict the coating deposition and pores formation, considering the influences of particle size, velocity, temperature and location related to the substrate on the coating properties by process modeling.

5.2 Coating Buildup in Thermal Spraying

The quality of thermal spray coatings is directly determined by size, velocity, temperature, and melting status of sprayed particles before they impact on the substrate. Plasma jets typically exhibit high temperatures and velocities; steep gradients of temperature, velocity and composition; and a variety of temporal fluctuations. In order to produce higher-quality coatings and expand the use of this versatile family of technologies, the ability to model and measure particle behaviours during in-flight and deposition is essential. To make the model useful for the coating property prediction, it is important to consider thermal spray processes from plasma generation to coating buildup. An advanced coating buildup model based on three sub-models, the plasma-particle model, splat formation model and coating buildup model will be integrated to predict the coating property evolution and microstructure.

5.2.1 Plasma and Particle In-flight Model

The short exposure times of particles to these flow fields and rapid deceleration and solidification of the particles upon impact give rise to a number of complicated non-equilibrium conditions. A reliable description of transport phenomena involved in the process is therefore essential. During plasma spraying, carrier gas and powders are usually injected into the plasma jet, as shown in Figure 5.1 (a). Three-dimensional effects thus always exist, and may appreciably affect the behaviors of the plasma flame and injected particles. It is anticipated that the plasma jet will be deflected from its original geometrical axis due to the transverse injection of carrier gas and particles. This deflection will affect the coating formation. Powder particle size distribution is another important parameter for the coating property control.

A comprehensive three-dimensional computational code (LAVA3D-P) was developed at Stony Brook recently and will be used to predict the plasma flame formation, flame- particle interaction, and particle state and trajectory. A typical coating microstructure picture is shown in Figure 5.1 (b). Computational particles are stochastically generated by sampling from probability distributions of particle properties at the point of injection. Each computational particle represents a group of similar physical particles. Particle trajectory, thermal history and stochastically distribution can be calculated simultaneously with the motion of the flame gas. The detailed description of the plasma flame and particle in flight model can be found in Xiong's paper (Xiong, Zheng et al. 2004). The model treats the plasma as a compressible, continuous multi-component, chemically reacting ideal gas with temperature-dependent thermodynamic and transport properties. The ionization, dissociation, recombination, and other chemical

reactions are treated using a general kinetic algorithm. The particle was modelled as discrete Lagrangian entities that exchange mass, momentum, and energy with the gas.

Here the particle model will be briefly introduced. The movement of particles is driven by the drag force due to the velocity difference between the particle and gas. For $\mathrm{Re}_\rho < 100$, the drag coefficient can be expressed as:

$$C_D = \frac{F_D}{A_f\left(\frac{1}{2}\bar{\rho}\Delta V^2\right)} = \left(\frac{24}{\mathrm{Re}_p} + \frac{6}{1+\sqrt{\mathrm{Re}_p}} + 0.4\right) f_{prop}^{-0.45} f_{Kn}^{0.45} \tag{5-1}$$

where ΔV is the velocity difference between the gas and the particle; f_{prop} and f_{Kn} represent the effects of variable plasma properties and non-continuum, respectively. To develop a particle heating and melting model, we assume that the particle is spherical and the internal convection within the molten part of the particle is negligible. Particles are heated up or cooled down by the surrounding gas by heat convection or radiation. A one-dimensional heat-conduction equation that considers the phase change will be solved numerically using a coordinate transformation and finite-difference method. The temperature distribution inside the particle is determined by:

$$\rho_p C_p \frac{\partial T}{\partial r} = \frac{1}{r^2}\frac{\partial}{\partial r}\left(k_p r^2 \frac{\partial T}{\partial r}\right) \tag{5-2}$$

where the subscript represents the particle properties. The melting interface is treated as an internal moving boundary between two different phase domains. The boundary conditions are given as $T_i = T_m$ and

$$\left(k_p \frac{\partial T}{\partial r}\bigg|_{r=r_m^-}\right) + \left(k_p \frac{\partial T}{\partial r}\bigg|_{r=r_m^+}\right) = \rho_p L \frac{dr_m}{dt} \tag{5-3}$$

The interface velocity is related with the energy balance at the interface.

Using the model of plasma and particle in-flight, we can obtain the particle size (D), velocity (V), temperature (T) and trajectory (x, y, z) before it impacts on the substrate. The particle parameter distribution on the substrate can be simplified as normal distribution as follows:

$$g(P) = \frac{1}{\sigma\sqrt{2\pi}} \exp\left(-\frac{1}{2\sigma^2}(P-\beta)^2 \right) \quad \textbf{(5-4)}$$

where: $\bar{P}$ is the mean value and σ is the standard deviation. By analyzing numerical data, we can obtain the statistical distribution of the particles, e.g., mean value and standard deviation. It is noted that such information can also be obtained from the experiments through particle diagnostic. In fact, the prediction by numerical model has been compared with the experimental data. A good agreement is obtained. Due to the presence of the substrate, gas velocity and particle movement might deviate from the free jet results. At this stage, we assume that the effects of the existing substrate on plasma flame and particle behaviors negligible.

5.2.2 Splat Formation Model

At impact, particle size, velocity, temperature, and molten fraction, along with substrate temperature and roughness control the splat morphology and consequently determine the microstructure of the coating. When a molten or partially melted droplet is in contact with a cold substrate or previously deposited layer, a high rate of heat transfer from the splat to the substrate will lead to a significant melt undercooling near the substrate. Crystalline nuclei nucleate on the substrate surface followed most of the time by columnar growth. Depending on the heat transfer and solidification conditions, either

planar or cellular growth or both may be possible during solidification, leading to very different microstructures. Also, not all particles will stick to the substrate during impact; particles may bounce off from the substrate. The deposition efficiency is dependent of the interplay among particle kinetic energy, dissipation energy, surface tension energy and solidification. It will be very useful for developing a formulation, which is a function of the Reynolds number, surface characteristics and melting status, Weber number and Stefan number, for the prediction of the deposition efficiency, particle morphology, microstructure, and adhesion. The process becomes much more complicated when a particle impacts on the surface with highly complex topology. Based on many simplifications, several numerical models have been developed to correlate the particle and substrate characteristics with splat formation and the Reynolds and Sommerfeld numbers, melting index and oxidation index are developed to analytically correlate the particle and substrate characteristics with splat deposition efficiency, flattening ratio, and fragmentation degree.

Theoretically, it is possible to develop a coating buildup model based on the pipeup of thousands sample splats similar to the plasma-particle model. However, the detailed modelling of droplets spreading and solidification requires solving the flow of free liquid surfaces, motion of a liquid-solid-air contact line, wall adhesion, fluid instability, non-equilibrium solidification and interaction with other deposited splats. The model should be able to predict the high velocity impingement, droplet deformation, wall adhesion, rapid solidification, thermal stress, and microstructure formation. Although tremendous progress has been made, current computer power can only solve splat formation and interaction of very few splats. In this paper, simplified splat formation models will be

used to calculate the splat morphology from particle characteristics and substrate conditions. We will assume that all particles will stick on the substrate or deposited layer, particles are fully melted and splats are disk like shape.

Several theoretical models are available to predict the flattening ratio for a molten particle impacting on a slat substrate. The most famous one is the model proposed by Madjeski (Madejski 1976) and the flattening ratio ξ is related to the Reynolds number of the impacting particle,

$$\xi = a\,\mathrm{Re}^{0.2} \tag{5-5}$$

where a=1.2941 is used. The effects of the substrate conditions and solidification are not included in his model. Zhang *(Zhang 1999; Zhang, Wang et al. 2001)* has modified the Madjeski model based on the macroscopic mechanical energy balance among the kinetic energy, dissipation energy, surface tension energy and solidification. The analytical formulation of splat flattening ratio can be written as follows,

$$\xi = \left[\sqrt{\frac{Ja}{2\,\mathrm{Pr}}\frac{k_s}{k_l}+1}-\sqrt{\frac{Ja}{2\,\mathrm{Pr}}\frac{k_s}{k_l}}\right]^{-0.4}\left(1.18\,\mathrm{Re}^{0.2}\right) \tag{5-6}$$

where the Jacob number $Ja = c_p\left(T_m - T_B\right)/h_f$, Prandtl number $\mathrm{Pr} = \nu/\alpha = \mu/\left(\rho\alpha\right)$, and the bottom temperature of the splat T_B is estimated by:

$$T_B = \frac{k_l T_l/\sqrt{\alpha_l} + k_{sub}T_{sub}/\sqrt{\alpha_{sub}}}{k_l/\sqrt{\alpha_l} + k_{sub}/\sqrt{\alpha_{sub}}} \tag{5-7}$$

In Eqs. (5-6), the coefficient of 1.18 is obtained as the result of a higher-order velocity profile used in their model to estimate the kinetic energy and dissipation energy. Also solidification and substrate properties are considered in the model. However,

surface tension, substrate roughness and energy loss due to particle impact have been neglected. Both models can be used to predict the splat flattening ratio for partially stabilized zirconia droplets deposited on a stainless steel substrate. In this paper, the model proposed by Zhang et al. will be used.

5.2.3 Coating Build-Up Model

Thermal spray microstructures are composed of splat-based elements formed through impact and solidification of micro-sized droplets. The splat-based microstructures create a variety of imperfections, which can vary in size, volume density, morphology and orientation. Three principal defect types are present in the system: disk-like lamellar pores, which are formed due to imperfect intersplat wetting, leading to the decreased adhesion between the sprayed layers; globular pores formed as the result of lack of filling of the solidifying splat; and vertical microcracks in the splat and deposit which contribute to very fine porosity in ceramics. These defects and their related anisotropies affect modulus, fracture toughness, strain hardening, etc., as well as functional attributes, such as, thermal conductivity. The dominant parameters for the coating formation and the resulting coating characteristics are the particle characteristics and substrate conditions, e.g., temperature, surface morphology, roughness, and oxidation. Depending on the shapes of splats and the nature of their interactions, different types of microstructure, varying porosities, and consequently different coating properties are obtained.

There is also a significant difference between ceramic coatings and metallic coatings. For ceramic coatings, curling plays an important role in the formation of coatings; the coating buildup mostly depends on the splat morphology of individual splat and the parameters distribution. For metallic coatings the SEM pictures of metallic coatings show that void occurs whenever the oxide layer appears. Particle oxidation during in-flight and splat oxidation during cooling are both important for metallic coating buildup. The existence of an oxide layer influences not only the porosity but also the thermal conductivity of the coatings. Different coating build-up models are therefore needed for ceramic and metallic coatings, due to different microstructure and mechanism. In this chapter, we will only focus on the ceramic coatings.

When a ceramic droplet arrives at the substrate or previously deposited layer, it interacts with the substrate/deposits, spreads and forms a liquid film. Heat is extracted from the film and droplet film starts to solidify because the substrate temperature is much lower than that of the droplet. The coating is periodically reheated by subsequently incoming particles. During the layering, the substrate temperature is one of the key parameters that will be measured. A low substrate temperature will result in splats with poor adhesion but low quenching and expansion-mismatch stresses. A high substrate temperature will improve the adhesion of splats and cohesion of the coatings, but the residual stresses may become too high. Based on the statistical distribution of droplets impacting on the substrate and splat formation, the splat layering process will be developed. Due to low thermal conductivity of the ceramic splat, the temperature difference across the splat thickness may be large. A temperature gradient is established through the splat thickness. After the splat is solidified the bottom of the splat is

constrained by the substrate/pre-deposited layer, and the quenching stress is developed in the splat. As a result of stress relief, curling of the splat edge may occur due to the interplay between the adhesion and stress. Splat curling will generate porosity in the deposit (Cirolini, Harding et al. 1991). We will consider this phenomenon as the major cause of the porosity formation in the final coating.

A 3-D stochastic model for thermal spray coating formation has been developed based on the mean values and standard deviations of droplet size, velocity, temperature, and impact point obtained from 3D simulations of particle and plasma interaction. The degree of splat edge curl up can be calculated. Based on probability density function, we can estimate the instantaneous process parameters of each impacting particle and calculate the splat geometry. Particles will be assumed to spread after impact and to form disks whose edges are curled up due to thermal stresses. The model will be used to predict coating porosity, thickness and roughness as a function of spray parameters.

The splat-based microstructures create a variety of imperfections, which can vary in size, volume density, morphology and orientation. A stochastic coating buildup model will be developed together with three-dimensional in-flight particle/plasma interaction. As shown in Figure 5.2 a splat on a flat substrate or pre-deposited layer, the lift gap δ can be estimated for free curling(Jiang 2000):

$$\delta = C\frac{D^2\gamma\left(T_l - T_{sub}\right)}{8\alpha} \qquad \textbf{(5-8)}$$

where D is the splat diameter before curling; C is a constant; T_l is the droplet temperature; T_{sub} is the substrate/pre-deposited layer temperature; α is the thermal diffusion of the splat; γ is the thermal expansion coefficient of the splat.

In the experiments, most splats cannot undergo free curling. A large portion of splat is in good adhesion with substrate or previously deposited layer. Stress can only curl the poorly adhered edge part away. We use a contact factor to account for this constrained curing:

$$\delta = C\frac{D^2\gamma\left(T_l - T_{sub}\right)}{8\alpha}\left(1-f\right) \qquad \textbf{(5-9)}$$

As shown in Figure 5.2. It varies between 0 for free curling and 1 for complete constrained case.

In spray experiment, adhesion depends on spray technique/particle/substrate conditions. Usually the contact factor is high for metallic deposit and low for ceramic coating. It is difficult to quantify the influence of spray parameters and particle and substrate conditions on the contact factor. Here we will investigate the influence of different adhesion (contact factor) on the coating properties.

Experimental studies on thin single splats have shown that the splashing of the splats is more complex than what has been suggested by the model. The splat may not be a perfect disk and it may have an irregular shape. It is clear that more detailed models of splat-splat interaction are desirable in the future. Nevertheless, as we shall see, even a model as simple as the one presented here can lead to convinced representation of the structure of the coating. In our model we assume the splat is a disk-like shape and curling up after cooling down. We also assume that the substrate is a rigid metal surface at a constant temperature. The splats form the coating by assembling them one by one. There are a few set of rules to model this process:

(1) The program assumes that the droplet follows exactly the shape of the under layer where it is under the impact region of the coming particle.

(2) If the top layer under the splat is not flat, there will be a displacement of the centre of the splat; the displacement depends on the maximum height difference of the region under the splat, as shown in Figure 5.3 (a).

(3) The splat will curl up provided that it is the topmost layer (shown in Figure 5.2). The total amount of curling is estimated as a function of distance from the impact region using Equation (5-9).

(4) The void will not be filled if it is not on the top surface.

(5) A gap in the surface narrower than the height of the splat will not be filled, but forms a globular pore as shown in Figure 5.3 (b).

Three-dimensional Cartesian grids are used to define the computational domain and to track the shape and position of the coating surface. The z coordinate lies in the plane of the substrate and the y axis is perpendicular to it. The structure of the coating is defined using a variable known as the 'volume fraction' ($F_{i,j,k}$), which is a ratio of the cell volume V_{cell} to the cell occupied by coating material V_m,

$$F_{i,j,k} = V_m / V_{cell} \quad \textbf{(5-10)}$$

where, $F_{i,j,k}$ equals unity when the cell is filled with coating material and zero when the cell is empty. For a partially filled cell $0 < F_{i,j,k} < 1$, a case when the cell is at the coating boundary or contains a part of a pore. A splat is generated in the model from a particle whose volume, temperature and location are specified, knowing together with the impact

conditions. The volume fraction is defined in the computational grids by computing the fraction of mass volume occupying the cell at coordinates (i, j, k) using:

$$F_{i,j,k} = \frac{1}{\Delta x_i \Delta y_j \Delta z_k} \int_{\Delta x_i} \int_{\Delta y_j} \int_{\Delta z_k} F_{i,j,k} dx dy dz \qquad \textbf{(5-11)}$$

5.3 Results and discussion

5.3.1 Droplet parameters

Using the LAVA3D-P program, we can obtain the particle parameters at impact. For droplets, the corresponding impact location (x, z), the average droplet velocity, temperature and diameter at that location and the variation are shown in Table 3. These data will be used to predict the final splat geometry from Eqs. (5-6) and (5-7). The splat location can be determined by the impact location on the substrate surface. The ZrO_2 particle is used in the plasma and particle in–flight model and its properties of are listed in Table 4.

Table 3 Droplet parameters

Parameters	Velocity (m/s)	Diameter (μm)	Temp. (K)
Mean Value	178.4	26.5	3157
Stand. Dev. (z=-1.4~-0.4cm)	16.1	3.6	98.4

* Droplet number: 5000; substrate size: 10mmx10mm.

Table 4 ZrO_2 particle conditions

Feeding rate, (kg/hr)	1.2	$C_{p,l}$, J/kg-K	713
Average size(μm)	30	ρ_s, g/cm^3	5.89
Stand distance(mm)	100	ρ_l, g/cm^3	5.89
k_s, W/m-K	2.0	T_m, K	2950
k_l, W/m-K	3.0	L_m, kJ/kg	812.4
$C_{p,s}$, J/kg-K	580	L_{evap}, kJ/kg	6000

5.3.2 Splat parameters

Once the droplet parameter already generated by LAVA3D-P program, we can get the splat morphology before curling up. As shown in Figure 5.4 (a) and (b), the analytical correlation for ZrO_2 droplets fits closely to numerical results for different droplet size and velocities. The results are also in good agreement with the flattening ratio measured by

Jiang (Jiang, Matejicek et al. 1999)for Zirconia on steel. While the curve for Mo droplets significantly lower than the Madjeski's prediction and closer to experimental results. The discrepancy comes from the validity of the isothermal assumption for the substrate. For ZrO_2 droplets on steel this assumption matches well with the fact that the thermal diffusivity of ZrO_2 is much smaller than that of steel. But for Mo-Steel, it is obvious that the isothermal assumption is not accurate because of high thermal conductivity of both splat and substrate, the isothermal assumption is not applicable at all. For ceramic droplet we can use Majeski's model to simply the prediction of splat morphology, but when it comes to the metallic droplet, Zhang's model will be more accurate.

Eqs. (5-6) and (5-7) will be used in the coating buildup model to predict the ceramic splat morphology before curling up happens. The total amount of curling is estimated as a function of distance from the impact region using Equation (5-9). That is the splat shape before it impacts with the substrate or the former deposited layer.

5.3.3 Coating structures

The coating deposition is simulated. We assumed that droplet impacts, and deforms on the substrate and forms laminar structure following the coating buildup rule list in section 5.2.3. As a result of deformation of one particle after another, layer by layer deposition will be formed.

A two-dimensional model is applied to the deposition of ZrO_2 particles. Figure 5.5 shows a typical plasma sprayed coating obtained by simulations. In this figure, Y is the

direction of coating buildup and the white spots represent the pores in the coatings, where the contact factor *f*=0.5.

To simulate this process, the grid size of 1000x1000 is used to cover the entire droplet. This ensures the grid size is sufficient small to resolve the regional resolution for the droplet shape. For droplets, first a random number is generated and based on the data by LAVA-3D simulation. The corresponding impact location (x, z) is obtained as well. Once (x, z) is determined, the average droplet velocity, temperature and diameter at that location will be evaluated. These data will then be used to predict the basic splat geometry from Eqs. (5-6) and (5-7). The splat location can be determined by the impact location on the substrate surface. For the coating buildup model we can obtain the coating properties: average thickness, roughness and porosity in the cross-section.

The model predicts that the porosity decrease with increasing the droplet impacting velocity. Assume the average coating thickness is *Ym*, the average coating roughness is estimated by:

$$R = \frac{1}{Z_0}\int_0^{Z_0} |Y - Ym| dZ \qquad \textbf{(5-12)}$$

Figure 5.6 shows the variation of the coating porosity with the mean value of velocity. Figure 5.7 and Figure 5.8 shows the variation of coating average thickness and the surface roughness when the droplets mean velocity changes. For different contact factors f = 0.4, 0.5, 0.6, 0.7 and 0.8, which represent the contact condition between splat and pre-deposited layer, the coating porosity, average thickness and roughness variation are showed in Figure 5.9, Figure 5.10 and Figure 5.11 respectively. Other particle

parameters used in the simulations are present in Table 4. The simulation results show that the larger the contact factor, the less the porosity of the coating. Certainly the coating average thickness will decrease because the volume of the pore inside the coating decreases when the contact factor decreases.

From the coating porosity, thickness and roughness, we observe that the coating properties are directly related to the droplet parameters; but the droplet parameters are related to the spray parameters. The spray parameters therefore can be linked to the coating properties. Figure 5.12 shows the morphology of the predicted coating when a 3D coating buildup model is used.

In the 3D coating buildup simulation, the mesh size of 100 × 100 × 300 is used and the particle number of 1000 is assigned. The coating section views at three different locations are shown in Figure 5.13. From results we can clearly observe the porosity of the coating; we can also analyze the coating in the same way as shown in Figure 5.4-Figure 5.11. The coating average porosity, thickness and roughness can therefore be obtained.

5.4 Conclusions

We have simulated the thermal spray coating process to predict the coating microstructures related to the spray parameters. The coating properties such as coating porosity, coating thickness, surface roughness are predicted by integration of the plasma-

particle, splat formation, and coating buildup models. The coating properties such as porosity, average thickness and average roughness were investigated as a function of process parameters. The current model has severe restrictions due to many assumptions. However, results demonstrate that even with such an idealized description of interaction between splats, the model can be used to generate fairly realistic coating properties. The current model forms a foundation for further improvement of an advanced ceramic coating build-up model.

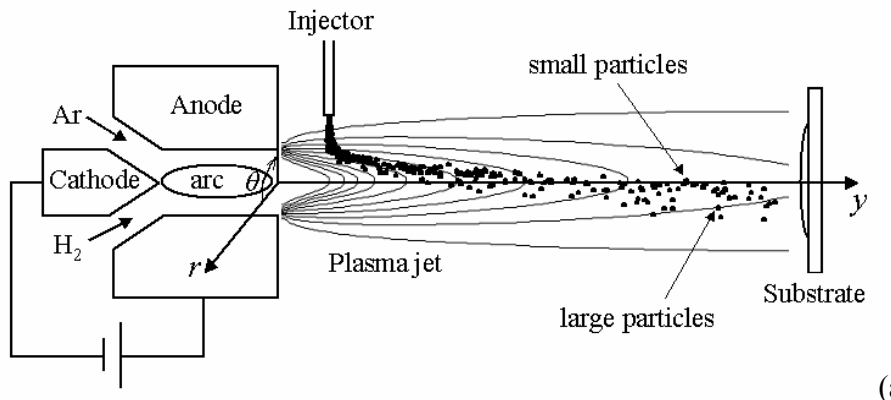

(a)

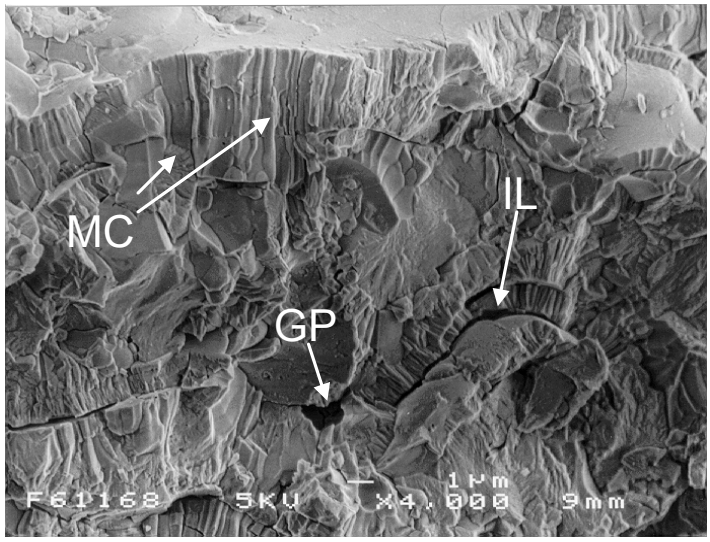

(b)

Figure 5.1 (a) Schematic of plasma spraying process; (b) Typical plasma sprayed

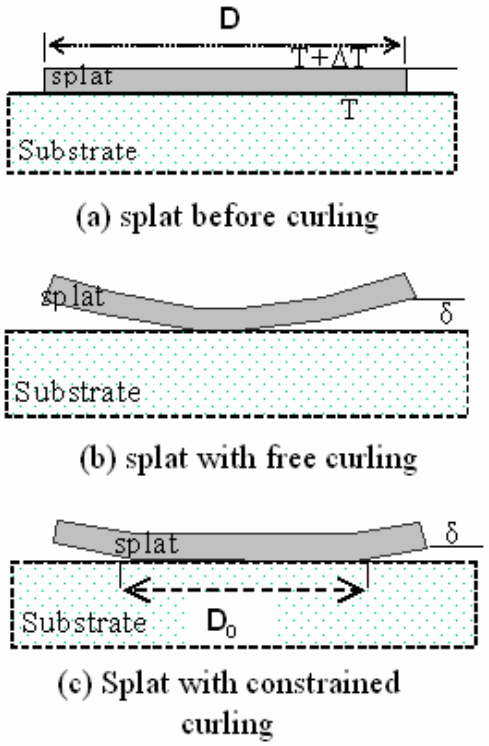

Figure 5.2 Schematic of splat shape before and after curling up

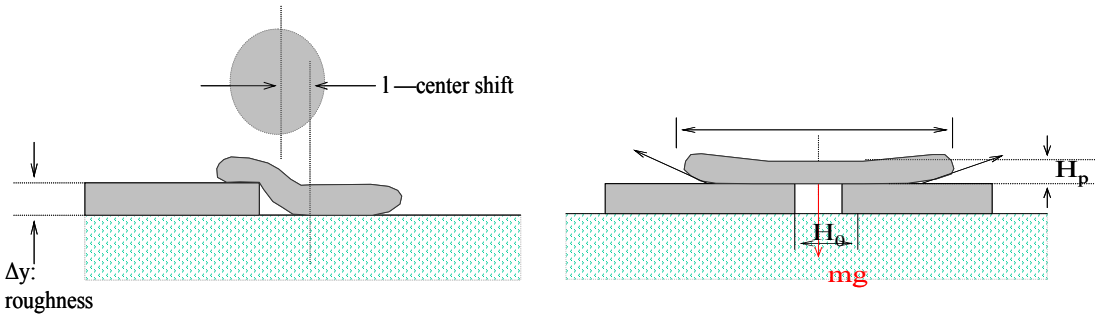

(a) (b)

Figure 5.3 Schematic of splat/splat interaction during coating buildup

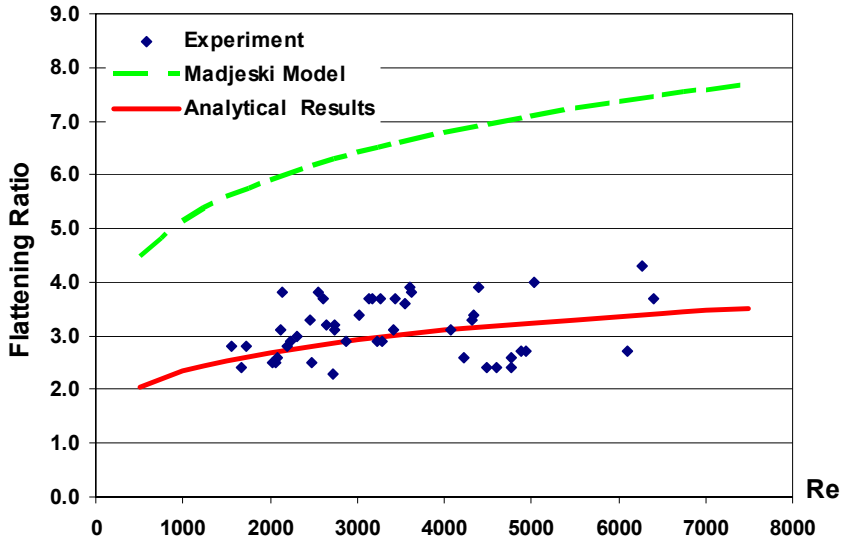

(a)

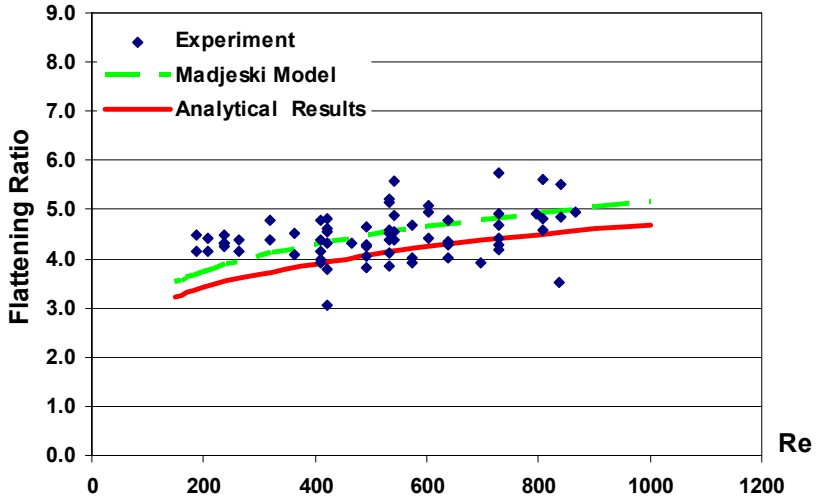

(b)

Figure 5.4 Flattening ratio Results from experiment, Madjeski Model and our analytical model as function of Reynolds number for (a) Mo splat on Stainless Steel (b) Zirconia on Stainless Steel

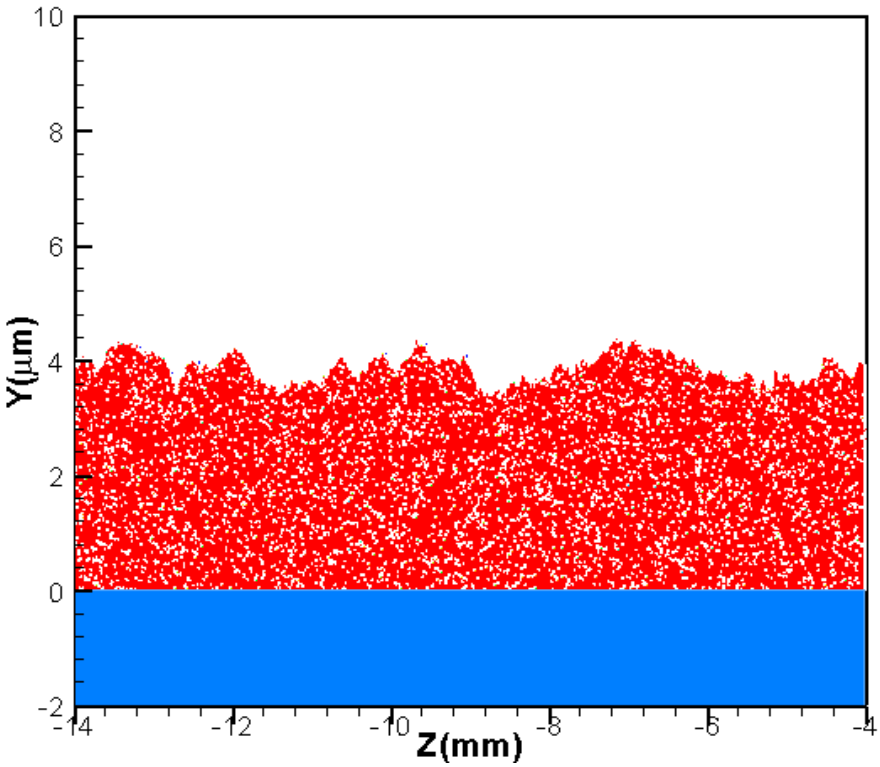

Figure 5.5 Typical coating structure produced by simulation

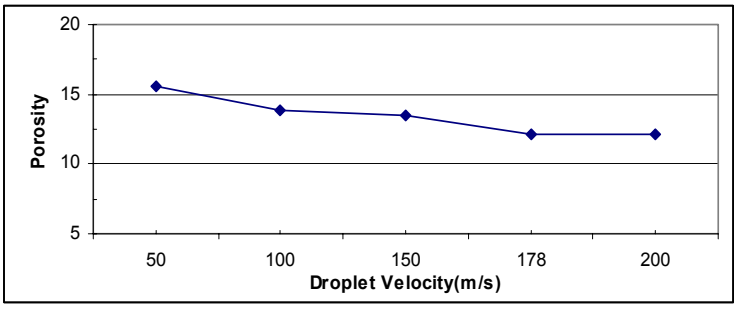

Figure 5.6 Porosity of coating vs. droplet mean velocity

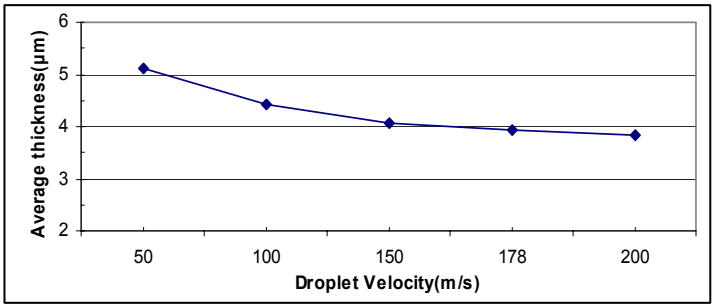

Figure 5.7 Thickness of coating vs. droplet mean velocity

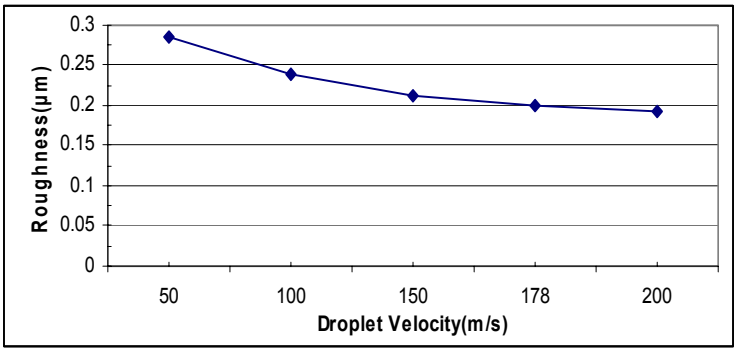

Figure 5.8 Roughness of coating vs. droplet mean velocity

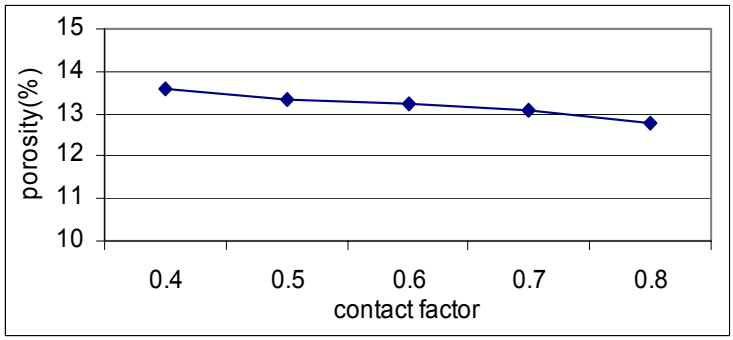

Figure 5.9 Porosity of coating vs. contact factor

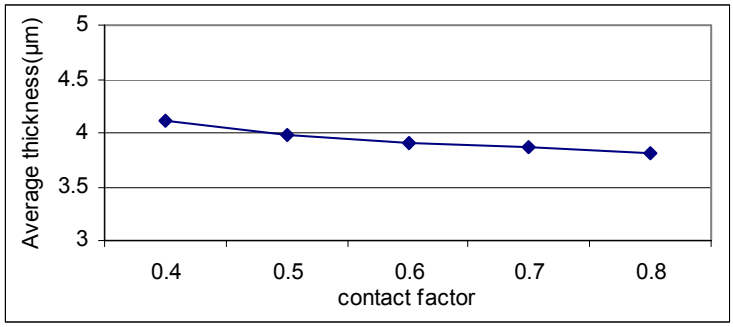

Figure 5.10 Thickness of coating vs. contact factor

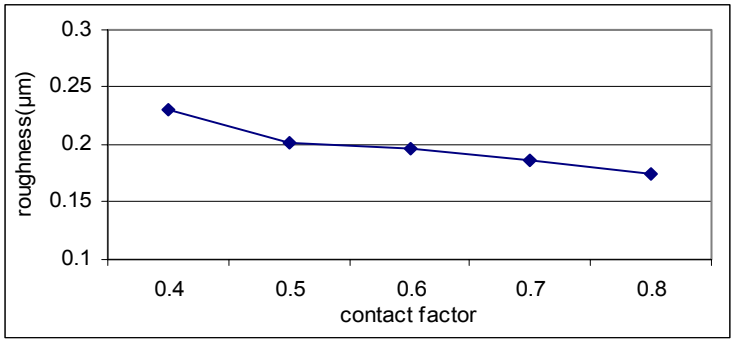

Figure 5.11 Roughness of coating vs. contact factor

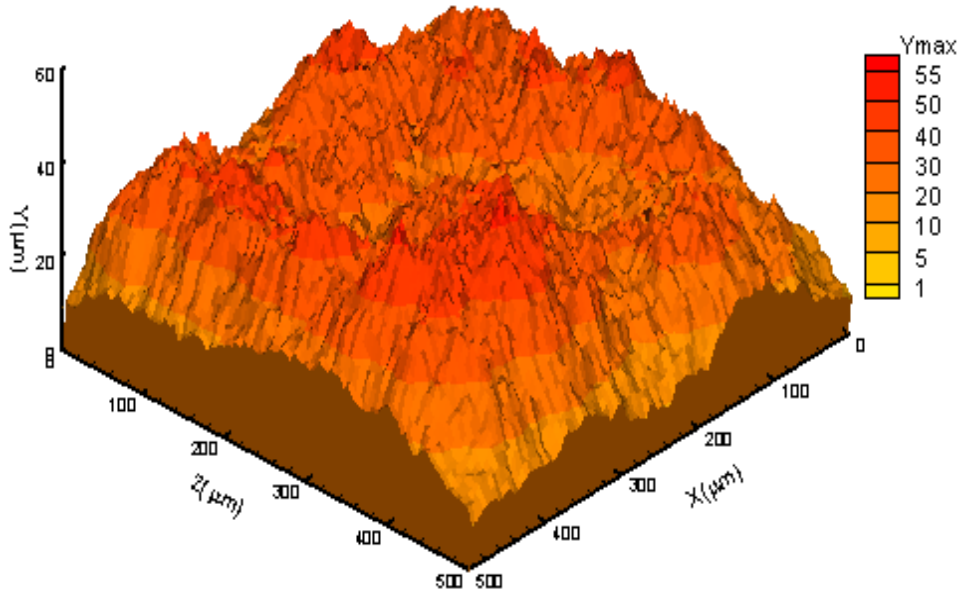

Figure 5.12 Simulated 3-D morphology of the coating

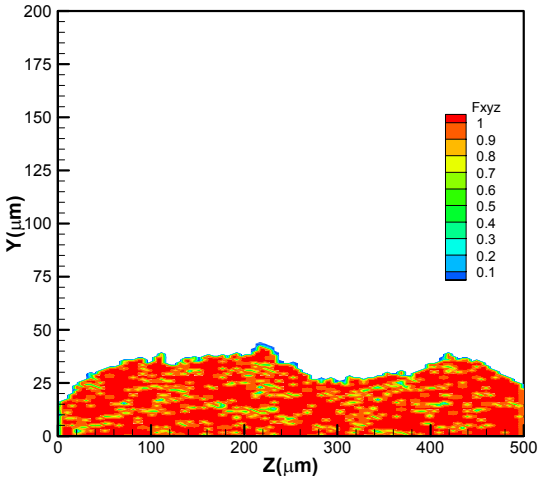

(a)

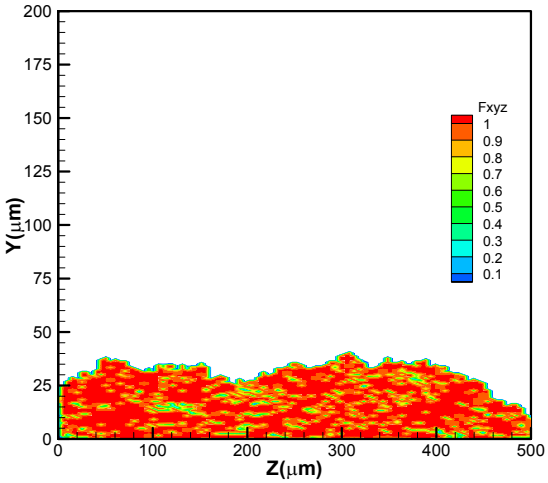

(b)

Figure 5.13 Three–dimensional simulation of the ZrO_2 coating: two cross section views: (a) Cross-section at X= 121.2μm; (b) Cross-section at X=247.5μm

Chapter 6 Summary and Suggestions for Future Work

6.1 Summary

This thesis aims to investigate heat and mass transfer for particle in flight, droplet deposition, and coating buildup. Numerical models have been developed to establish the quantitative relationship between the spray parameters, particle/substrate materials and deposition characteristics. Modeling study will focus on the melt flow during particle in-flight for particles with different morphologies, its influence on the drag force on the surface, and its influence on the particle/droplet morphology before/after impacting on the substrate. The coating deposition model focuses on three parts: splat formation, splat/substrate interaction and pileup of the splats.

6.1.1 Particle In-Flight Simulation

The level set method is used to simulate the droplet in-flight and spreading at impact. The level set function will be used to track the free surface deformation. The model is used to study the melt flow inside the droplet, deformation of the droplet, and instability for particles with different morphologies. The melt flow in the droplet and

deformation of the free surface will be calculated for different droplets. The effects of droplet size, velocity and morphology in the particle shape deformation and droplet spreading will be investigated.

6.1.2 Substrate Melting and Re-Solidification

A numerical model is developed to calculate substrate melting and re-solidification when a molten droplet impacts on a substrate. This model has been used to calculate the temperature history and the solid/liquid interface location. For a given material pair, substrate melting and re-solidification are investigated. Simulation results reveal that initial splat and substrate temperatures play the important roles on the maximum melting depth of the substrate and thus on the bonding of the coatings. The results also confirm that imperfect contact or interfacial heat transfer coefficient will have a significant influence on substrate melting and re-solidification. Substrate melting and re-solidification also depends on thermal physical properties of the materials. From analysis, a dimensionless parameter, temperature factor, has been proposed and can be used as an indicator whether a substrate melting will occur for a certain combination of the droplet and substrate, and it can be correlated with the maximum melting depth of the substrate. A design is proposed to heat up the substrate by the plasma gun together with a cooling device attached at the backside of the substrate, by which the substrate front surface temperature can be controlled at a sufficient high temperature. With additional heating from superheated molten droplets and the latent heat of droplet solidification, a thin layer of the substrate will be melted and epitaxy growth of the splats is possible.

6.1.3 Coating Build-Up

The coating properties such as coating porosity, coating thickness, surface roughness are predicted by integration of the plasma-particle, splat formation, and coating buildup models. A comprehensive three-dimensional computational code (LAVA3D) will be used to predict the plasma flame formation, flame and particle interaction, and particle state and trajectory. Mean values and standard deviations of particle size, velocity, and temperature, and impact position are obtained from in-flight particle simulations. These spray parameters controlled droplet characteristics together with the given substrate conditions will be used as initial conditions of splat morphology predictions and in turn as the input for coating buildup. We proposed a set of coating build-up rules to predict coating deposition and formation of the pores, considering the influences of particle size, velocity, temperature and location related to the substrate. The current model has severe restrictions due to many assumptions. However, results demonstrate that even with such an idealized description of the interaction between splats, the model can be used to generate fairly realistic coating properties. The current model forms a foundation for further improvement of an advanced ceramic coating build-up model.

6.2 Suggestion for Future Investigation

The following areas of research are suggested:

6.2.1 Particle In-Flight

- Improve the program to study hollowed particle deformation: use finer grid and improve the mass conservation, using particle level set method.
- Entrapped air will result in many voids in the splat center. Such voids are undesirable since they will lead to porosity increase and strength reduction in the coating. There is also concern that air trapped under splats will prevent them from adhering well, consequently coating quality is degraded. Numerical model can be used to study the air trapping phenomena observed in thermal spraying.
- Study the air-droplet-substrate interaction to investigate the instability of the droplet in flight and impact, which will help to reveal the formation of droplet wave-patterned structure at the top and wave-patterned adhesion zone at the bottom.
- Include the heat transfer into the level set method to simulate the solidification of the droplet. For droplet spreading, solidification plays an important role, especially for metallic particles. It is essential to consider its effect on the splat morphology, which is the element of the entire coating microstructure and properties.

6.2.2 Substrate Melting and Re-Solidification

- Melting and re-solidification of the substrate plays an important role in thermal spray coating. Through the modeling study, it is possible to establish a relationship

between the bonding strength with substrate melting. It will be very useful to quantity this relationship for forming the better coatings..

- Another issue is that we studied the substrate melting for the first layer deposition. If we can build a substrate melting map for the particles and substrates used in thermal spraying, that will help to understand the coating bonding characteristics, furthermore people could use it to classify whether there is substrate melting, how much it is and related issues.
- We studied the first layer splats impacting on the substrate. For splats on the former deposited layers, we can use the same method to study the bonding between the splat layers.
- With the substrate temperature control device we can get substrate melting by heating up the substrate by the plasma gun together with a cooling device attached at the backside of the substrate to make epitaxy growth of the splats possible. Further improvement of this technique to use in practice. It can be used in several applications, for example, in electronics and magnetic materials. However, powders used in such applications are usually more complicated for modeling. We selected a simple material combination to prove the concept. We will also be able to perform experimental studies in the future. For YSZ on stainless steel itself, a bond coating may be a better solution for better adhesion.

6.2.3 Coating Build-Up

There are still several restrictions in the model. Improvement is necessary.

- The coating buildup model is based on the splat morphology of individual splat and stochastic distribution. However coating buildup mechanisms are different for different coatings. For ceramic coatings, from microstructure we see that there are four important parts: interlamellar pores, globular pores, microcracks, and macrocracks. Splat curling plays an important role in the formation of ceramic coatings. During the splat solidification, the bottom of the splat is constrained by the substrate/pre-deposited layer; quenching stress is developed in the splat. As a method of the stress relaxing, curling of the splat edge will occur. For metallic coating. The SEM pictures of NiAl coatings show that void occurs whenever the oxide layer appears, interpreted as representing incomplete contact between the splats and the underlying oxide. Particle oxidation during in-flight and splat oxidation during cooling are both important for coating buildup. The existence of an oxide layer influences not only the porosity but also thermal conductivity of the coating. The metallic coatings buildup model can also be developed based on the input data from analysis, modeling and experiments.
- Improve rules of the coating growth. The influences of partially melted particle, cracks in the ceramic coating and oxides on the metallic coating buildup should be considered.

Reference

Amon, C. H., K. S. Schmaltz, et al. (1996). "Numerical and Experimental Investigation of Interface Bonding via Substrate Re-melting if an Impinging Molten Metal Droplet." Journal of Heat Transfer **118**: 164-172.

Attinger, D. and D. Poulikakos (2001). "Melting and Resolidification of Substrate Caused by Molten Microdroplet Impact." Journal of Heat Transfer **123**: 1110-1122.

Boulos, M. I., P. Fauchais, et al. (1994). Thermal Plasmas, Fundentals and Applications. New York, Plenum Press.

Boulos, M. I., P. Fauchais, et al. (1993). Fundamentals of Plasma Particle Momentum and Heat Transfer, Singapore: World Scientific.

Chang, Y. C., T. Y. Hou, et al. (1996). "A Level Set Formation of Eulerian Interface Capturing Methods for Incompressible Fluid Flows." Journal of Computational Physics **124**: 449-464.

Chen, S., B. Merriman, et al. (1997). "A Simple Level Set Method for Solving Stefan Problem." Journal of Computational Physics **135**: 8-29.

Chen, X. and E. Pfender (1983). "Behavior of small particles in a thermal plasma flow." **3**(3): 351-366.

Chen, Y., G. Wang, et al. (2001). "Numerical simulation of coating growth and pore formation in rapid plasma spray tooling." Thin solid film **390**: 13-19.

Chung, M. and R. H. Rangel (2001). "Parametric study of metal droplet deposition and solidification process including contact resistance and under cooling effects." International Journal of heat and mass Transfer **44**: 605-618.

Cirolini, S., J. H. Harding, et al. (1991). "Computer Simulation of Plasma-Sprayed Coatings: I, Coating Deposition Model." Surface & Coatings Technology **48**: 137-145.

Clyne, T. W. (1984). "Numerical Treatment of Rapid Solidification." Metall. Trans. B **15B**: 369-381.

Dykhuizen, R. C. (1994). "Review of Impact and Solidification of Molten Thermal Spray Droplets." J. of Thermal Spray Technology **3**: 351-361.

Dyshlovenko, S., L. Pawlowski, et al. (2006). "Modelling of plasma particle interactions and coating growth for plasma spraying of hydroxyapatite." Surface and Coatings Technology **200**(12-13): 3757-3769.

Fauchais, P. (2004). "Understanding Plasma Spraying." Journal of Physics D: Applied Physics **37**: R86-R108.

Fauchais, P., J. F. Coudert, et al. (1992). "Diagnostics of thermal spraying plasma jets." Journal of Thermal Spray Technology **1**: 117-128.

Fauchais, P., A. Vardelle, et al. (2001). "Quo Vadis Thermal Spraying?" Journal of Thermal Spray Technology **10**(1): 44-66.

Fukumoto, M. and Y. Huang (1999). "Flattening Mechanism in Thermal Sprayed Nickel Particle Impinging on Flat Substrate Surface." J. Thermal Spray Technology **8**(3): 427-432.

Hansbo, A. and P. Nylen (1999). "Models for the Simulation of Spray Deposition and Robot Motion Optimization in Thermal Spraying of Rotating Objects." Surface and Coating Technology **122**: 191-201.

Harten, A., B. Engquist, et al. (1987). "Uniformly High-Order accurate Essentially Non oscillatory Schemes, III." J. Compute Phys. **71**: 231-303.

Herman, H. and S. Sampath (1996). Chapter 10: Thermal Spray Coatings. In book: Metallurgical and Ceramic Protective Coatings. K. H. Stern, Chapman & Hall, New York, NY**:** 261-289.

Hermanek, F. J. (2001). Thermal Spray Terminology and Company Origins. ASM International. Materials Park,OH.

Jiang, X. (2000). Deposit Formation Dynamics and Microstructure Development during Thermal Spraying. Materials Sciences and Engineering. Stony Brook, NY 11794, State University of New York at Stony Brook.

Jiang, X. Y., J. Matejicek, et al. (1999). "Substrate Temperature Effects on the Splat Formation, Microstructure Development and Properties of Plasma Sprayed Coatings, Part II: Case Study for Molybdenum." Materials Sci. Eng. **A272**: 189-198.

Klocher, T. and T. W. Clyne (2001). Process Modeling to Optimise the Structure of Hollow Zironia Particle for Use in Plasma Sprayed Thermal Barrier Coatings. ITSC, Singapore, ASM.

Klocher, T. and T. W. Clyne (2003). "In Flight Behavior of Dense and Hollow Particles during Plasma Spraying: Part I - a Numerical Model." J. Ther. Spray, Tech.

Klocher, T. and T. W. Clyne (2003). "In Flight Behavior of Dense and Hollow Particles during Plasma Spraying: Part II -Experimental Study." J. Ther. Spray, Tech.

Knotek, O. and R. Elsing (1987). "Monte Carlo Simulation of the Lamellar Structure of Thermallly Sprayed Coatings." Surface and Coatings Technology **32**: 261-271.

Kulkarni, A., Z. Wang, et al. (2003). "Comprehensive microstructural characterization and predictive property modeling of plasma-sprayed zirconia coatings." Acta Materialia **51**(9): 2457-2475.

Lavernia, E. J. and N. J. Grant (1988). "Spray Deposition of Material: A Review." Mat. Sci. Eng. **98**: 381-394.

Li, C. J., C. X. Li, et al. (2006). Examination of Substrate surface Melting Induced Splashing during Splat Formation in Plasma Spraying. International Thermal Spray Conference & Exposition, Seattle Washington USA, May 15-17, 2006.

Li, L., X. Y. W. Wang, G., et al. (2004). "Substrate Melting during Thermal Spray Splat Quenching." Thin Solid Films **468**(1-2): 113-119.

Li, M. and P. D. Christofides (2005). "Multi-scale modeling and analysis of an industrial HVOF thermal spray process." Chemical Engineering Science **60**(13): 3649-3669.

Li, M. and P. D. Christofides (2005). "Multi-scale Modeling and Analysis of an Industrial HVOF Thermal Spray Process." Chemical Engineering Science **60**: 3649-3669.

Lugscheider, E., C. Barimani, et al. (1996). "Modeling og APS Plasma Spray Process." Computational Materials Science **7**: pp. 109-104.

Madejski, J. (1976). "Solidification of Droplets on a Cold Surface." Int. J. Heat Mass Transfer **19**: 1009-1013.

Mariaux, G., E. Legros, et al. (2003). Modeling of Coating Formation and Heat Flux to Substrate by Particle and Plasma Jet in Plasma Spraying. Thermal Spray 2003: Advancing the science & Applying the Technoligy, Materials Park, Ohio, USA, ASM International.

McPherson, R. (1981). "The relationship between the mechanism of formation, Microstructure and propertied of plasma-sprayed coating." Thin Solid Film **83**: 297-310.

Montavon, G. and C. Coddet (1996). "Quantification of Particle Morphology in View of Quality Control of the Thermal Spray Process." Materials Characterization **36**: 257-269.

Mostaghimi, J., S. Chandra, et al. (2003). "A. Dolatabadi, Modeling thermal spray coating processes: a powerful tool in design and optimization." Surface and coating techniligy **163-164**: 1-11.

Ohta, M., T. Imura, et al. (2005). "A Computational Study of the Effect f Initial Bubble Conditions on the Motion of a Gas Bubblr Rising in Viscous Liquids." International Journal of Multiphase Flow **31**: 223-237.

Osher, S. and J. A. Sethian (1988). "Fronts Propagating with Curvature Dependent Speed: Algorithms Based on Hamilton-Jacobi Formulation." Journal of Computational Physics **79**(1): 12-49.

Pasandideh-Fard, M., R. Bhola, et al. (1998). "Deposition of tin droplets on a steel plate: simulations and experiments." International Journal of Heat and Mass Transfer **41**(19): 2929-2945.

Pasandideh-Fard, M., S. Chandra, et al. (2002). "A Three-Dimensional Model of Droplet Impact and Solidification." International Journal of Heat and Mass Transfer **45**: 2229-2242.

Sampath, S. and H. Herman (1996). "Rapid Solidification and Microstructure Development during Plasma Spray Deposition." Journal of Thermal Spray Technology **5**(4): 445-456.

Sethian, J. A. (1999). Level Set Methods and Fast Marching Methods: Evolving Interfaces in Computational Geometry, Fluid Mechanics, Computer Vision, and Materials Science. New York, Cambridge.

Sethian, J. A. and P. Smereka (2003). "Level Set Methods for Fluid Interfaces." Annu. Rev. Fluid Mech. **35**: 341-372.

Shanmugavelayutham, G., V. Selvarajan, et al. (2006). "In-flight particle behaviour and its effect on co-spraying of alumina-titania." Current Applied Physics **6**(1): 41-47.

Shi, D., M. Li, et al. (2004). "Diamond Jet Hybrid HVOF Thermal Spray: Rule-Based Modeling of Coating Microstructure." Ind. Eng. Chem. Res. **43**: pp. 3653-3665.

Sobolev, V. V. and J. M. Guilemany (1995). "Prediction of powder particle behavior during high-velocity oxyfuel spraying." Journal of Thermal Spray Technology **4**(3): 287.

Steffens, H. D., B. Wielage, et al. (1991). "Interface Phenomena and Bonding Mechanism of Thermally-Sprayed Metal and Ceramic Composites." Surf. Coat. Technol. **45**: 290-308.

Sussman, M., A. S. Almgren, et al. (1999). "An Adaptive Level Set Approach for Incompressible Two-Phase Flows." Journal of Computational Physics **148**: 81-124.

Sussman, M., P. Smereka, et al. (1994). "A Level Set Approach for Computing Solution to Incompressible Two-Phase Flow." Journal of Computational Physics **114**: 146-159.

Vardelle, M., A. Vardelle, et al. (1995). "Influence of Particle Parameters at Impact on Splat Formation and Solidification in Plasma Spraying Processes." Journal of Thermal Spray Technology **4**(1): 50-58.

Waldvogel, J. M. and D. Poulikakos (1997). "Solidification Phenomena in Picoliter Size Solder DropletDeposition on a Composite Substrate." Int. J. Heat Mass Transfer **40**(2): 295-309.

Wan, Y. P., V. Prasad, et al. (1999). "Model and Powder Particle Heating, Melting, Resolidification, and Evaporation in Plasma Spraying Processes." Journal of Heat Transfer-Transactions of the ASME **121**: 691-699.

Wan, Y. P., H. Zhang, et al. (2001). "Role of Solidification, Substrate Temperature and Reynolds Number on Droplet Spreading in Thermal Spray Deposition: Measurements and Modeling." Journal of Heat Transfer **124**(4): 382-389.

Wang, G.-X. and E. F. Matthys (2002). "Experimental Determination of the Interfacial Heat Transfer during Cooling and Solidificaiton of Molten Metal Deoplets Impacting on a Metallic Substrate: Effect of Roughness and Superheat." International Journal of Heat and Mass Transfer **45**: 4967-4981.

Wang, G. X. and E. F. Matthys (1992). "Numerical Modeling of Phase Change and Heat Transfer during Rapid Solidification Processes: Use of Control Volume Integral with Element Subdivison." Int. J. Heat Mass Transfer **35**: 141-153.

Wang, G. X. and E. F. Mattys (1996). On the Heat Transfer at the interface between a Solidifying Metal and a Solid Substrate, in Melt-Spinning, Strip casting, and Slab casting. TMS Pub., Warrendale, PA.

Wang, G. X., V. Prasad, et al. (1997). "An Interface-tracking Numerical Method for Rapid Planar Solidification of Binary Alloys with Application to Microsegregation." Materials Science and Engineering A **225**: 47-58.

Wang, G. X., V. Prasad, et al. (2001). "Rapid Solidification in Tthermal Spray Deposition: Microstructure and Modeling." Sadhana **26**: 35-37.

Wang, S.-P., G. X. Wang, et al. (1998). "Melting and re-solidification of a substrate in contact with a molten metal: Operational maps." Int. J. Heat Mass Transfer **41**: 1177-1188.

Wang, X. (2002). Modeling of Rapid Solidification, Splat Morphology, and Melt Flow during Thermal Spraying. Materials Sciences and Engineering. Stony Brook, NY 11794, State University of New York at Stony Brook.

Wang, X. Y., H. Zhang, et al. (2002). "An Integrated Model for Interaction between Melt Flow and Non-Equilibrium Solidification in Thermal Spraying." International Journal of Heat and Mass Transfer **45**: 2289-2301.

Xiong, H., L. L. Zheng, et al. (2004). "Three -Dimensional Simulation of Plasma Spray: Effect of Carrier Gas Flow and Particle Injectionon Plasma Jet and Entrained Particle Behavior." International Journal of Heat and Mass Transfer **47**: 5189-5200.

Xu, D.-Y., X.-C. Wu, et al. (2003). "Motion and Heating of Non-Spherical Particle in a Plasma Jet." Surf. Coat. Technol. **171**: 149-156.

Zhang, H. (1999). "Theoretical Analysis of Spreading and Solidificaiton of Molten Droplet during Thermal Spray Deposition." International Journal of Heat and Mass Transfer **42**: 2499-2508.

Zhang, H., X. Y. Wang, et al. (2001). "Studies of Splat Morphology and Rapid Solidification during Thermal Spraying." Int. J. Heat Mass Transfer **44**: 4579-4592.

Zhang, H., X. Y. Wang, et al. (2004). "Numerical Simulation of Nucleation, Solidification, and Microstructure formation in Thermal Spraying." International Journal of Heat and Mass Transfer **47**: 2191-2203.

Zhang, H., L. L. Zheng, et al. (1998). "A Curvilinear Level Set Formation for Deformable Free Surface Problems with Application to Solidification." Numerical Heat Transfer B **34**: 1-20.

Zhao, H.-K., B. Merriman, et al. (1998). "Capturing the Behaviour of Bubbles and Drops Using the Variational Level Set Approach." J. Comput. Phys. **143**: 495-518.

Zheng, L. L. and H. Zhang (2000). "An Adaptive Level Set Method for Moving - Boundary Problems: Application to Droplet Spreading and Solidification." Numerical Heat Transfer B **37**: 437-454.